Molecular Dynamics Study of Polarizability Anisotropy Relaxation in Aromatic Liquids and Its Connection with Local Structure

M. Dolores Elola* and Branka M. Ladanyi*

Department of Chemistry, Colorado State University, Fort Collins, Colorado 80523

Received: April 3, 2006; In Final Form: June 1, 2006

The collective polarizability anisotropy dynamics in a set of three aromatic liquids, benzene (Bz), hexafluorobenzene (HFB), and 1,3,5-trifluorobenzene (TFB), has been studied by molecular dynamics simulation. These liquids have very similar shapes, but different electrostatic interactions due to opposite polarities of C−H and C−F bonds, giving rise to different local intermolecular structures in the liquid phase. We have investigated how these structural arrangements affect polarizability anisotropy dynamics observed in optical Kerr-effect (OKE) spectroscopy. We have modeled the interaction-induced polarizability with the first-order dipole-induced dipole approximation, with the molecular polarizability distributed over the carbon sites. Local contributions to the librational OKE spectrum were computed separately for molecules participating in parallel or perpendicular relative orientations within the first coordination shell. We found that the relative locations of parallel and perpendicular librational bands of the OKE spectra are closely related to the corresponding pair energy distributions of the closest four neighbors of a given molecule, corresponding to a model of a harmonic oscillator in a cage of nearest neighbors. This model predicts higher librational frequencies for more attractive intermolecular interactions, which in all three liquids correspond to parallel local arrangements. On the diffusive orientational time scale, all three liquids exhibit slower relaxation of molecules in parallel arrangements, although the difference in relaxation rates is substantial only in TFB, which has the strongest tendency toward parallel stacking. The analysis of the collective polarizability relaxation was performed using two different approaches, the projection scheme (*J. Chem. Phys.* **1980**, *72*, 2801) and the theory developed by Steele (*Mol. Phys.* **1987**, *61*, 1031) for the second time derivatives applied to collective time correlations. Both approaches allow the decomposition of the OKE response into contributions from orientational relaxation and other dynamical processes. We find that they lead to different predictions on how the response depends on collective reorientation and processes arising from fluctuations in the interaction-induced polarizability. We discuss the reasons for these differences and the advantages and disadvantages of the two analysis schemes.

I. Introduction

Studies of the dynamics and structure of aromatic liquids have been the subject of intense investigation for many years. Experimental measurements using neutron and X-ray diffraction techniques show that the average molecular arrangement in liquid benzene and hexafluorobenzene is similar to that in the solid, namely, neighboring molecules are oriented preferentially perpendicular to each other.[1−3] This feature has also been confirmed by molecular dynamics (MD) simulations.[4−7] A detailed analysis of the local order from the radial-angular pair correlation functions obtained from simulations shows that parallel and perpendicular arrangements coexist between pairs of molecules within the first coordination shell in both liquids. However, although perpendicular arrangements of neighboring molecules are preferred in benzene, parallel alignment within the first coordination shell are slightly favored in hexafluorobenzene.

In addition to similar shapes, benzene (Bz) and hexafluorobenzene (HFB) molecules have nearly the same polarizabilities and polarizability anisotropies (see Table 1).

However, there are significant differences in the molecular charge distributions due to the fact that the C−H and C−F bonds have opposite polarities. A consequence of this fact is that the electric quadrupole moments of Bz (-2.90×10^{-39} C m^2) and HFB (3.17×10^{-39} C m^2) are roughly equal in magnitude but opposite in sign.[8] The quadrupole−quadrupole interaction favors a perpendicular arrangement of neighboring molecules, whereas the dispersion interactions tend to favor parallel stacking. Thus, both arrangements are possible for neighboring molecules in the liquid phase, as indicated above. In the case of 1,3,5-trifluorobenzene (TFB), alternating C−H and C−F bonds give rise to a much smaller quadrupole, 0.31×10^{-39} C m^2, than those of Bz and HFB (ref 9); hence, the contributions of higher multipole moments will not be negligible, and then it is reasonable to presume that the structure of liquid TFB should be different from that of the other two liquids. Indeed, neutron diffraction experiments and molecular dynamics simulations[10−12] reveal that the short-range local order in TFB involves dimers in which the TFB molecules have a parallel stacked configuration over an average separation of less than 4 Å. This is consistent with the expectation that electrostatic interactions will favor parallel alignment of C−H and C−F bonds of neighboring molecules. Therefore, Bz, TFB and HFB form an interesting set of molecules in which the effect of local order on intermolecular dynamics can be investigated.

Information about the dynamics of intermolecular modes in a liquid can be obtained experimentally from depolarized

* To whom correspondence should be addressed. E-mail: dolores@colostate.edu; Branka.Ladanyi@colostate.edu.

10.1021/jp062071b CCC: $33.50 © 2006 American Chemical Society
Published on Web 07/14/2006

Rayleigh scattering (DRS) and nonlinear optical techniques, such as femtosecond optical heterodyne-detected Raman-induced Kerr-effect spectroscopy.[13−15] The time-dependent signal detected in these experiments is related to the time correlation function (TCF) of the many-body polarizability anisotropy of the system, which can in turn be computed easily from computer simulations.

It is now well known that polarizability anisotropy relaxation is a collective phenomenon, which has contributions from both the intrinsic or molecular, $\mathbf{\Pi}^{M}$, and interaction-induced, $\mathbf{\Pi}^{I}$, polarizabilities,[16−20] the former relaxing basically through reorientations and the latter by rotational and translational motions. In condensed phases, both contributions are usually important and must be taken into account.[21−25] As a result, both rotational and translational mechanisms are involved in the total relaxation.

There have been many attempts in the literature to separate the contributions from rotations and translations to polarizability relaxation, with the complication that there is also a nonnegligible cross rotation-translational coupling term contributing to the total signal. The separation into translational and rotational contributions can be achieved using the projection scheme first proposed by Keyes and Kivelson,[26] and implemented for the first time in MD simulations by Frenkel and McTague.[18] In this scheme, the anisotropic polarizability of the system is decomposed into components along and orthogonal to the anisotropic portion of the molecular polarizability, $\mathbf{\Pi}^{M}$.

Another scheme that has been useful in distinguishing between contributions from translational and rotational dynamics to the polarizability anisotropy relaxation is the approach developed by Steele.[27] In this case, the starting point is the polarizability anisotropy *velocity*. This quantity can be obtained from the polarizability through the chain rule of differentiation, and its rotational and translational components are proportional to angular and center-of-mass velocities, respectively.[28]

Ryu and Stratt[29] explored the OKE spectrum of benzene by MD simulation and instantaneous normal-mode (INM) analysis. Within the linear version of INM theory of dynamics in liquids, the identification of different dynamical mechanisms contributing to OKE is based on the analysis of the influence spectrum of the polarizability velocity. Rotational and translational components are obtained by projecting the polarizability derivatives with respect to normal coordinates into translational and rotational contributions.[22,30−32] At short times, for which the INMs provide an exact representation of the polarizability velocity TCF, the INM and Steele theory separations of the TCF into rotational, translational, and their cross-correlation components are equivalent. In this sense, the approach proposed by Steele[27] is closely related to INM analysis and can be considered an extension of the INM approach to longer times. By separating the responses arising from rotational and translational degrees of freedom, Ryu and Stratt showed that the unusual shape of the experimental benzene OKE spectra, also common to some other liquids of aromatic molecules,[33−38] (i.e., exhibiting a flat region at intermediate frequencies) arises from the presence of an especially large ratio of rotational to translational bandwidths. The large rotational bandwidth is due, in turn, to the planarity of the molecules, which requires that the moment of inertia for spinning is the sum of tumbling moments of inertia.

Inspired by Ryu and Stratt's work, Loughnane et al.[39] studied the set of liquids Bz-HFB-TFB by ultrafast optical OKE spectroscopy, as a function of temperature. On the basis of the influence of molecular parameters on the shape of the reduced OKE spectrum, they propose a model that links the different features of the OKE librational spectra to the local ordering. They assume, first, that the librational frequencies of the molecules depend on whether individual molecules participate in parallel or perpendicular arrangements. Because benzene is the liquid in this set with the greatest degree of perpendicular order and it also has the greatest intensity in the high-frequency region, they assume, second, that local perpendicular structures have higher librational frequencies than parallel ones.

In this work, we study the polarizability anisotropy relaxation in a set of aromatic liquids, Bz, HFB, and TFB, by MD simulations. We analyze the contributions from rotational and translational degrees of freedom to the collective dynamics, using two different approaches, namely, the projection scheme and the Steele theory applied to the second time derivative of the TCFs. We also focus on the model proposed by Loughnane et al.,[39] and we try to determine how the shape of the OKE spectra is related to the local structure in these liquids.

The remainder of this paper is organized as follows: in Section II we summarize the definitions needed for the computation of the polarizability anisotropy TCF, along with a detailed description of both schemes to separate orientational and translational contributions, namely, the projection scheme of Frenkel and McTague, and the Steele theory. Section III offers details of the simulation and describes the potential models used in this work. In Section IV, we briefly show the main characteristics of the local structure in these liquids, and in Section V the results obtained for the polarizability relaxation itself are presented and discussed. The two different schemes for separating the rotational and translational contributions to the polarizability anisotropy relaxation are also compared and discussed in Section V. The paper is concluded in Section VI with a summary of our main findings.

II. Theoretical Background

A. Polarizability Anisotropy Relaxation. The many-body polarizability, $\mathbf{\Pi}$, of a liquid composed of optically anisotropic molecules, is the dynamical variable whose fluctuations give rise to light scattering. For depolarized light scattering and for OKE, the dynamics of interest arise from the fluctuations in the polarizability anisotropy and can be related to the TCF of an off-diagonal element of the many-body polarizability tensor

$$\psi_{xz}(t) = \langle \Pi_{xz}(0)\, \Pi_{xz}(t) \rangle / \Gamma^2 \tag{1}$$

where Γ^2 is the depolarized light scattering intensity, that is, $\psi_{xz}(0)$, of a noninteracting system containing the same number and types of molecules as the system of interest. For pure liquids composed of N rigid molecules, it is given by $\Gamma^2 = N\gamma_0^2/15$, with γ_0^2 being the squared isolated-molecule polarizability anisotropy.

OKE is a measurement of transient optical birefringence within the liquid and is due to electronic and nuclear responses to an optical field pulse. The portion of the OKE signal due to motion of the nuclei is referred to as the nuclear response function, $R(t)$, and is related to $\psi_{xz}(t)$ by

$$R(t) = -\beta \frac{\partial}{\partial t} \psi_{xz}(t) \tag{2}$$

where $\beta = 1/k_B T$ is the usual Boltzmann factor. The nuclear response can also be represented in the frequency domain, by performing a Fourier−Laplace transform of $R(t)$ according to

$$\chi(\omega) = \int_0^\infty e^{i\omega t} R(t)\, dt \tag{3}$$

where the imaginary part is the susceptibility, the spectral density for polarizability anisotropy relaxation

$$\chi''(\omega) \equiv \mathrm{Im}[\chi(\omega)] = \int_0^\infty \sin(\omega t)\, R(t)\, \mathrm{d}t \tag{4}$$

The collective polarizability tensor, $\mathbf{\Pi}$, for a molecular system in the condensed phase is usually expressed in terms of a permanent molecular (or intrinsic) contribution, $\mathbf{\Pi}^{\mathrm{M}}$, which, as will be seen later, depends on individual orientational variables, and an interaction-induced component, $\mathbf{\Pi}^{\mathrm{I}}$, that arises from the interactions among induced dipoles of different molecules. Within the first-order dipole-induced dipole (DID) approximation,[18,23,24] $\mathbf{\Pi}^{\mathrm{I}}$ is a pairwise additive quantity

$$\mathbf{\Pi} = \mathbf{\Pi}^{\mathrm{M}} + \mathbf{\Pi}^{\mathrm{I}} = \sum_i^N \boldsymbol{\alpha}_i + \sum_{i,j\neq i}^N \boldsymbol{\pi}(ij) \tag{5}$$

where $\boldsymbol{\alpha}_i$ represents the unperturbed gas-phase molecular polarizability. The DID approximation has often been implemented by considering molecular polarizabilities to be concentrated on the center of mass of each molecule.[18,23,29,40,41] This model is usually referred to as the center−center DID approach. For polyatomic molecules, this representation of $\mathbf{\Pi}^{\mathrm{I}}$ becomes inaccurate when the distances between molecules are not necessarily larger than intramolecular separations. The model may be improved by considering the intrinsic polarizability as distributed over a set of interacting sites within the molecule.[24,25,42−47] In this case, the first-order contribution to the interaction-induced polarizability between molecules i and j will be given by

$$\boldsymbol{\pi}(ij) \simeq \sum_{mn} \boldsymbol{\alpha}_{im} \cdot \mathbf{T}^{(2)}(\mathbf{r}_{im,jn}) \cdot \boldsymbol{\alpha}_{jn} \tag{6}$$

where $\boldsymbol{\alpha}_{im}$ is the effective polarizability of site m on molecule i and $\mathbf{T}^{(2)}(\mathbf{r})$ is the dipole tensor

$$\mathbf{T}^{(2)}(\mathbf{r}) = \frac{3\hat{\mathbf{r}}\hat{\mathbf{r}} - \mathbf{1}}{r^3} \tag{7}$$

with $\hat{\mathbf{r}} = \mathbf{r}/r$ and $\mathbf{1}$, the unit tensor. $\mathbf{r}_{im,jn}$ in eq 6 represents the vector between site m on molecule i and site n on molecule j. We will refer to this model as the site−site DID approximation.

In previous work on Bz/HFB mixtures[47] we found that the site−site DID model yielded better agreement with experimental data. We observed that the fact of distributing the polarizability over the sites of the aromatic ring has a stronger positive impact on the OKE spectrum of HFB than of Bz; this is probably related to the higher sensitivity of HFB to the distribution of sites in the molecular plane, because of the higher degree of parallel local order in HFB as compared to Bz. In view of the fact that in TFB the extent of parallel arrangements is even larger than that in HFB, we have employed the site−site model for describing interaction-induced contributions to the collective polarizability in the present work.

A polarizability tensor, $\boldsymbol{\alpha}$, with axial symmetry can be written as

$$\boldsymbol{\alpha} = \left[\gamma_0\left(\hat{\mathbf{u}}\hat{\mathbf{u}} - \frac{1}{3}\mathbf{1}\right)\right] + \bar{\alpha}\mathbf{1} \tag{8}$$

where the term in square brackets is the traceless component of rank $\neq 2$ (anisotropic) and $\bar{\alpha}\mathbf{1}$, the isotropic component, with $\bar{\alpha} = \mathrm{Tr}(\boldsymbol{\alpha})/3$, of rank $\neq 0$. The unit vector along the symmetry axis of the molecule is represented by $\hat{\mathbf{u}}$ in eq 8, and γ_0 is the scalar polarizability anisotropy, which for axially symmetric molecules takes the simple form $\gamma_0 = (\alpha_{\parallel} - \alpha_{\perp})$, with $\alpha_{\parallel}$ and $\alpha_{\perp}$ the polarizability components along and perpendicular to the symmetry axis, respectively.

TABLE 1: Polarizability Components (in Å^3) for Isolated Molecules: $\alpha_{\parallel}$ and $\alpha_{\perp}$ are the Components along and Perpendicular to the Symmetry Axis; $\bar{\alpha}$ and γ_0 Represent the Isotropic and Anisotropic Polarizabilities

liquid	$\alpha_{\parallel}$	$\alpha_{\perp}$	$\bar{\alpha}$	γ_0
Bz[a]	6.54	11.73	10.00	−5.19
HFB[b]	4.58	12.08	9.58	−7.50
TFB[c]	6.14	12.23	10.20	−6.90

[a] Reference 50. [b] Reference 51. [c] Reference 52.

To compute the interaction-induced collective polarizability (eq 6), we need a model to obtain the effective polarizabilities $\boldsymbol{\alpha}_{im}$. As in our previous work on polarizability relaxation in Bz/HFB mixtures,[47] here we are using a simple site−site scheme proposed by Mossa et al.[46] In this model, the molecular polarizability is distributed over the six carbon sites

$$\boldsymbol{\alpha}_{im} = \left[\gamma_{0,m}\left(\hat{\mathbf{u}}_i\hat{\mathbf{u}}_i - \frac{1}{3}\mathbf{1}\right)\right] + \bar{\alpha}_m\mathbf{1}\ (1 \le m \le 6) \tag{9}$$

In the case of Bz and HFB, each of the sites are assigned $^1/_6$ of the total molecular polarizability tensor, thus, $\gamma_{0,m} = \gamma_0/6$ and $\bar{\alpha}_m = \bar{\alpha}/6$.

For TFB, we considered it more realistic to assign different polarizabilities to carbon sites bound to hydrogen and those attached to fluorine atoms. An estimate of the ratios between the components of the CH and CF effective polarizabilities has been obtained using the Thole model;[48] once these ratios were known, they were used to obtain the appropriate effective CH and CF polarizabilities such that by adding them up the experimental molecular polarizability value for TFB is reproduced. Therefore, we first computed the polarizability tensor for the isolated TFB molecule within Thole's model, using the atomic parameters given in table 7 of ref 49. Then, the effective polarizabilities of the three CH and CF groups in the molecule, $\boldsymbol{\alpha}_{\mathrm{CH}}(m)$ and $\boldsymbol{\alpha}_{\mathrm{CF}}(m)$, have been computed by summing over the effective polarizabilities obtained for the corresponding C, H and C, F atoms. The sum of the three effective CH (or CF) polarizabilities, divided by three, gives an effective-site tensor, $^1/_3\sum_{m=1}^3 \boldsymbol{\alpha}_{\mathrm{CH}}(m) = \boldsymbol{\alpha}_{\mathrm{CH}}$, that has the same axial symmetry of the molecule. The components of $\boldsymbol{\alpha}_{\mathrm{CH}}$ and $\boldsymbol{\alpha}_{\mathrm{CF}}$ were found to satisfy the following relations

$$\frac{\alpha_{\mathrm{CF}}^{\parallel}}{\alpha_{\mathrm{CH}}^{\parallel}} \approx 1.05 \quad \text{and} \quad \frac{\alpha_{\mathrm{CF}}^{\perp}}{\alpha_{\mathrm{CH}}^{\perp}} \approx 1.24 \tag{10}$$

Because the model of eq 9 assumes that the total molecular polarizability is equal to the sum of the six terms, that is, the sum of all effective polarizabilities (and thus, it neglects intramolecular−DID interactions), the following conditions hold for the total parallel and perpendicular molecular polarizabilities

$$\alpha_{\parallel} = 3(\alpha_{\mathrm{CF}}^{\parallel} + \alpha_{\mathrm{CH}}^{\parallel})$$

$$\alpha_{\perp} = 3(\alpha_{\mathrm{CF}}^{\perp} + \alpha_{\mathrm{CH}}^{\perp}) \tag{11}$$

The values for the parallel and perpendicular polarizabilities of an isolated molecule of TFB were taken from experimental data, and are displayed in Table 1, along with the corresponding values used for Bz and HFB. The effective polarizabilities for CH and CF groups obtained by solving the set of eqs 10−11

yielded $\alpha_{CH}^{\parallel} = 1.00$ Å^3, $\alpha_{CH}^{\perp} = 1.82$ Å^3, $\alpha_{CF}^{\parallel} = 1.05$ Å^3, and $\alpha_{CF}^{\perp} = 2.26$ Å^3.

Inserting the expression 5 for the collective polarizability into $\psi_{xz}(t)$ (eq 1), this TCF becomes a sum of three contributions, namely, $\psi_{xz}^{MM}(t)$, $\psi_{xz}^{II}(t)$, and $\psi_{xz}^{MI}(t)$, the first two corresponding to molecular and induced polarizability autocorrelations and the third to their cross correlation. This natural separation of the polarizability anisotropy TCF is not always the most informative because it does not distinguish among different relaxation mechanisms that contribute to $\psi_{xz}(t)$. As will be shown in Section V, all three components are nonnegligible over the time scale depicted. Moreover, $\psi_{xz}^{MI}(t)$, which is in this case, as in many other fluids,[23,24,25,40,53] almost as large as $\psi_{xz}^{MM}(t)$, but of the opposite sign, decays at a similar rate as $\psi_{xz}^{MM}(t)$ does at long times. To separate $\psi_{xz}(t)$ into components that relax via collective reorientation from those that have a different dynamical origin, one can project Π_{xz}^{I} along Π_{xz}^{M} into a component that decays through reorientational dynamics and into an orthogonal component, Π_{xz}^{CI}, using a method that has been used and discussed in previous works.[18,20,23−25] The resulting polarizability components are then the reorientational (R) and collision-induced (CI) terms

$$\Pi_{xz}^{R} = (1 + f_{xz})\,\Pi_{xz}^{M} \tag{12a}$$

$$\Pi_{xz}^{CI} = \Pi_{xz}^{I} - f_{xz}\,\Pi_{xz}^{M} \tag{12b}$$

where $f_{xz} = \langle \Pi_{xz}^{M}\Pi_{xz}^{I}\rangle/\langle(\Pi_{xz}^{M})^2\rangle = {}^1/_2\psi_{xz}^{MI}(0)/\psi_{xz}^{MM}(0)$ is a time-independent renormalization factor for Π_{xz}^{M}.

B. Steele Theory Applied to Polarizability Dynamics. In the present case, the starting point of the approach proposed by Steele[27] is the collective polarizability velocity, $\dot{\mathbf{\Pi}}$. In the case of a fluid of rigid molecules, the collective polarizability of the system, given by eq 5, depends on two types of variables: the center-of-mass separation vectors, $\mathbf{r}_{ij}$, and the orientational unit vectors, $\hat{\mathbf{u}}_i$, of the molecules in the liquid. Therefore, the collective polarizability velocity, $\dot{\mathbf{\Pi}}$, which is given by the molecular and the interaction-induced components, $\dot{\mathbf{\Pi}} = \dot{\mathbf{\Pi}}^{M} + \dot{\mathbf{\Pi}}^{I}$, can also be expressed as a sum of translational and rotational contributions

$$\dot{\mathbf{\Pi}} = \dot{\mathbf{\Pi}}^{Tr} + \dot{\mathbf{\Pi}}^{Rot} \tag{13}$$

$\dot{\mathbf{\Pi}}^{Tr}$ and $\dot{\mathbf{\Pi}}^{Rot}$ are obtained by differentiating $\mathbf{\Pi}$ (via the chain rule) with respect to translational and rotational coordinates. The explicit expressions for the time derivatives of eq 13 within the center−center DID approximation can be found in refs 22, 28, 32, and 54. The derivation and the explicit expressions for $\dot{\mathbf{\Pi}}^{Tr}$ and $\dot{\mathbf{\Pi}}^{Rot}$ within the present version of the site−site DID model are given in Appendix A, and the expression for the time derivative of the site−site dipole tensor can be found in Appendix B. However, we note here that in the center-center model for $\mathbf{\Pi}^{I}$, the dipole tensor $\mathbf{T}^{(2)}(\mathbf{r})$ and its time derivative depend exclusively on intermolecular center-of-mass separations; whereas in the site−site approach, the dipole tensor depends on both center-of-mass and orientational coordinates of the pair involved. Thus, its time derivative will give rise to a translational contribution and an extra rotational one, which is absent from the center−center model.

The TCF of polarizability anisotropy velocity $\dot{\mathbf{\Pi}}$ can be written, by analogy with eq 1, as

$$G_{xz}(t) = \langle \dot{\Pi}_{xz}(0)\,\dot{\Pi}_{xz}(t)\rangle/\Gamma^2 \tag{14}$$

TABLE 2: Intermolecular Potential Parameters[a]

pair	B_{mm} (kJ mol^{-1})	C_{mm} (Å^{-1})	A_{mm} (kJ mol^{-1}Å^6)	q_m/e
C−C	369 743	3.60	2 439.8	−0.153[b] +0.120[c] +0.04727[d] −0.02787[e]
H−H	11 971	3.74	136.4	+0.153[b] +0.01847[f]
F−F	400 000	4.35	500.0	−0.120[c] −0.03787[f]

[a] Reference 4. [b] In benzene. [c] In hexafluorobenzene. [d] For C bound to F in 1,3,5-trifluorobenzene. [e] For C bound to H in 1,3,5-trifluorobenzene. [f] In 1,3,5-trifluorobenzene.

It can be naturally separated into three terms, $G_{xz}^{MM}(t)$, $G_{xz}^{II}(t)$, and $G_{xz}^{MI}(t)$, arising from the autocorrelations of molecular and induced polarizability velocities and the cross term between the two, or, alternatively, into rotational, translational, and rotation−translational coupling correlations

$$G_{xz}(t) = G_{xz}^{Rot}(t) + G_{xz}^{Tr}(t) + G_{xz}^{RotTr}(t) \tag{15}$$

Furthermore, it is straightforward to prove that $\psi_{xz}(t)$ and $G_{xz}(t)$ are related by

$$G_{xz}(t) = -\ddot{\psi}_{xz}(t) \tag{16}$$

This implies that $R(t)$, the nuclear response function (eq 2), which is proportional to the time derivative of the polarizability anisotropy TCF, is in turn proportional to the time integral of $G_{xz}(t)$

$$R(t) \propto -\dot{\psi}_{xz}(t) = \int_0^t G_{xz}(\tau)\,\mathrm{d}\tau \tag{17}$$

III. Potentials and Simulation Details

The potential model chosen to describe the intermolecular interactions in these liquids is the Williams potential,[55,56] in which the intermolecular potential energy between a pair of atoms is given by

$$\varepsilon_{mn}(r) = B_{mn}\exp(-C_{mn}r) - \frac{A_{mn}}{r^6} + \frac{q_m q_n}{4\pi\epsilon_0 r} \tag{18}$$

where m and n label the C, H, and F atoms and r is the distance between atoms m and n. Using this potential, each molecule was modeled as a rigid body with 12 interacting sites located on the atom positions. The first term in eq 18 accounts for short-range repulsion; the second term represents attractive dispersive interactions, and the last term is the Coulombic electrostatic contribution, where q_m represents the partial charge on site m. The values of the potential parameters were taken from ref 4 and are reproduced here in Table 2. As for the partial charges in TFB, we have chosen to employ the parameters corresponding to model I of ref 4, which reproduce the experimental quadrupole moment of an isolated molecule accurately. Bond lengths were taken as $d_{C-C} = 1.393$ Å, $d_{C-H} = 1.027$ Å, and $d_{C-F} = 1.320$ Å. Cross potential parameters for the pure liquids were calculated from the usual combination rules, $B_{mn} = (B_{mm}B_{nn})^{1/2}$, $C_{mn} = (C_{mm} + C_{nn})/2$, and $A_{mn} = (A_{mm}A_{nn})^{1/2}$.

The simulations were performed in the microcanonical ensemble at an average temperature of 298 K with a total of $N = 256$ rigid molecules placed inside a cubic box corresponding to the experimental density at that temperature, using density

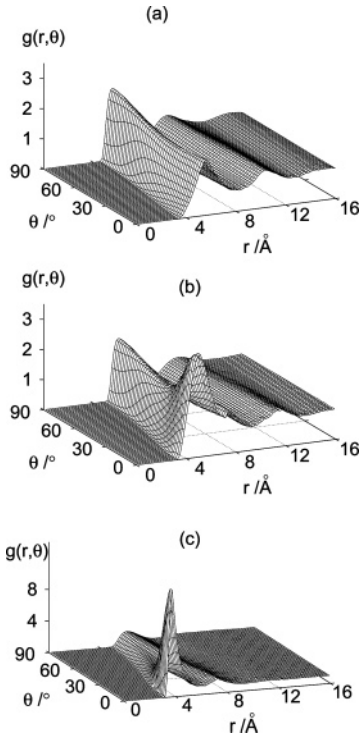

Figure 1. Radial-angular pair correlation function for (a) Bz, (b) HFB, and (c) TFB.

values of 0.874, 1.60, and 1.27 g/cm^3 for Bz, HFB, and TFB, respectively.[7,12,57] Short-ranged intermolecular interactions were cut off at half the box length, while standard Ewald sums with conducting boundaries were used to handle long-range Coulomb forces. The constraint method[58] was used to integrate the equations of motion of the rigid planar molecules, in combination with the Verlet algorithm,[59,60] with a time step of 5 fs. Intramolecular distances between the basic set of atoms were kept fixed by using the SHAKE iterative procedure.[61] Preliminary trajectories of ~100 ps were first run for equilibration at 298 K; after this period, the trajectories were saved and 2 ns runs were used for data analysis.

IV. Local Structure

A. Static Properties. Information on local structure in the investigated liquids can be obtained from the MD simulations using the radial center-of-mass pair correlation functions $g_{cm}(r)$, and with the help of the radial-angular pair correlation function $g(r,\theta)$, defined as

$$g(r,\theta) = \frac{1}{N\rho(r,\theta)} \langle \sum_{i \neq j}^{N} \delta(r - r_{ij})\, \delta(\theta - \theta_{ij}) \rangle \qquad (19)$$

$\rho(r,\theta)$ represents the number of molecules, defined as $(N/V)2\pi r^2 \sin\theta \Delta r \Delta\theta$, Δr and $\Delta\theta$ are the radial and angular resolutions, and r_{ij} and θ_{ij} are, respectively, the center-of-mass intermolecular distance and the angle between the sixfold axes of molecules i and j. The angular brackets indicate a time average. Angular and radial resolutions were taken as $\Delta\theta = 2°$ and $\Delta r = 0.01(L/2)$ respectively, with L being the simulation box length.

Pair correlations in these liquids have been studied extensively by Cabaço et al. in a range of thermodynamic states,[4,11,12,62] from room temperature up to supercritical conditions, using the same potential models. The main findings are summarized in the next paragraphs and illustrated in Figures 1−2.

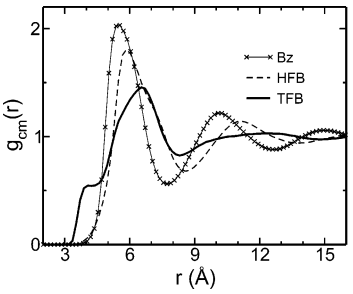

Figure 2. Radial pair correlation function between center of mass for Bz, HFB, and TFB molecules.

An almost isotropic local order is observed in Bz for distances greater than 5 Å, as seen in Figure 1a. At shorter separations, parallel arrangements seem to be slightly more favored for a better packing. A stronger tendency for parallel arrangements at short distances is found in HFB in Figure 1b, where $g(r,\theta)$ exhibits a clear maximum for $r \approx 5$ Å and $\theta = 0°$. Perpendicular configurations of molecules are found in HFB at slightly longer separations, around $r \approx 6$ Å. Thus, unlike in Bz, the probabilities of finding parallel and perpendicular configurations are out of phase: their maxima are located at different values of r. For these two liquids, there is a small likelihood of occurrence of stacked configurations at short distances.

The structure of TFB is substantially different from that of Bz and HFB. Indeed, $g(r,\theta)$ for TFB in Figure 1c exhibits a very intense peak at $r \approx 4$ Å and $\theta = 0°$, followed by a broad peak about 6.5 Å at small angles. The well-defined local structure in the range of 3.5−4.5 Å for small angles between pairs of molecules is not present in the other two liquids with such a high intensity, that is, $g(5.54$ Å, $0°) = 1.83$ in Bz, $g(5.12$ Å, $0°) = 3.39$ in HFB, and $g(3.71$ Å, $0°) = 13.54$ in TFB. There is a similar probability of finding pairs of molecules participating in parallel, intermediate, or perpendicular structures in Bz, whereas in HFB the first maximum of $g(r,\theta)$ for small angles is shifted toward smaller distances with respect to the corresponding peaks in $g(r,\theta)$ for larger angles. Figure 1c exhibits the signature of a stacked dimer structure in TFB, characterized by a very intense peak for $\theta = 0°$ centered at about 3.7 Å, corresponding to parallel arrangements. In this case the first maxima of the three slices of $g(r,\theta)$ corresponding to $\theta = 0$, 45, and 90° are not in phase, that is, they occur at different center-of-mass separations. Consequently, in Figure 2, where the center-of-mass radial pair correlation function for TFB is displayed, a pre-peak at about 4 Å can be appreciated, coming from the stacked structure of parallel molecules. The structure found in the 3.5−4.5 Å range of $g_{cm}(r)$ in this liquid has no counterpart in the other two fluids, as seen also in Figure 2.

The number of neighbors within a spherical shell of radius r, $N(r)$, can be computed by integrating the center-of-mass pair correlation function, $g_{cm}(r)$

$$N(r) = \rho \int_0^r g_{cm}(R) 4\pi R^2 \, dR \qquad (20)$$

where $\rho = N/V$ is the number density of the system. Moreover, a detailed separation of $N(r)$ in $N^{||}(r)$ and $N^{\perp}(r)$ could be obtained, depending on the average angle θ between symmetry axes of pairs of molecules. The superscripts || and ⊥ denote angular ranges of $0 \leq \theta \leq \pi/4$ and $\pi/4 < \theta \leq \pi/2$, respectively. These numbers can be calculated by integrating the radial-angular pair correlation function over the range of interest

$$N^{||}(r) = \rho \int_0^r \int_0^{\pi/4} 2\pi R^2 g(R,\theta) \sin(\theta)\, d\theta\, dR \qquad (21)$$

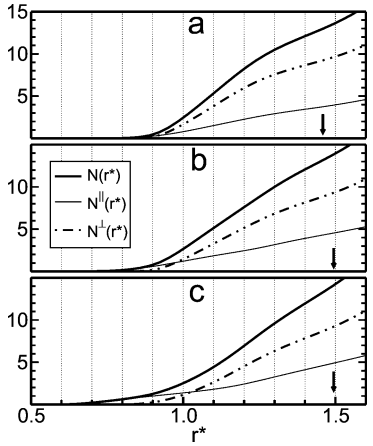

Figure 3. Coordination number $N(r^*)$ (bold solid line) as a function of the reduced distance $r^* = r\rho^{1/3}$, and coordination numbers for parallel and perpendicular arrangements, $N^{\parallel}(r^*)$ (−) and $N^{\perp}(r^*)$ (− · · −); for (a) Bz, (b) HFB, and (c) TFB molecules. Arrows indicate the position of the reduced radius corresponding to the first coordination shell.

TABLE 3: First-Shell Coordination Radius (D_1) and Average Number of Neighbors in the First Shell (N_1), along with $N_1^{\parallel}$ and $N_1^{\perp}$ (see the text)

liquid	D_1/Å	N_1	$N_1^{\parallel}$	$N_1^{\perp}$
Bz	7.73	12.77	3.75 (30%)	9.02 (70%)
HFB	8.60	13.47	4.49 (33%)	8.98 (67%)
TFB	8.31	13.57	4.74 (35%)	8.83 (65%)

with a similar expression for $N^{\perp}(r)$, but integrating the angular variables between $\pi/4$ and $\pi/2$. Figure 3 displays the coordination number, $N(r)$, for the three liquids studied, where we found it more representative to use the reduced distance $r^* = r\rho^{1/3}$, defined in terms of the liquid density, ρ, following Cabaço et al. in ref 4. Figure 3 shows that $N^{\parallel}(r^*)$ is larger than $N^{\perp}(r^*)$ only at very small reduced separations, below $r^* \approx 0.9$. At smaller values of r^*, the number of perpendicular neighbors is negligible; the largest value of $N^{\parallel}$ at $r^* = 1$ corresponds to TFB, which is equal to 1.44. It can also be seen that in TFB, $N^{\parallel}(r^*)$ starts growing up at smaller r^* than for the other two fluids, consistently with the existence of the pre-peak found in $g_{cm}(r)$. At larger separations, the main contribution to $N(r^*)$ is given by the neighbors that are arranged in perpendicular configurations.

Table 3 displays the radius of the spherical first coordination shell, corresponding to the location of the first minimum in the radial pair distribution function $g_{cm}(r)$, depicted in Figure 2, along with the number of neighboring molecules found in the first shell, N_1, or classified depending on the angle formed between the symmetry axes, $N_1^{\parallel}$, $N_1^{\perp}$, obtained from Figure 3. Consistent with Figures 1−3, benzene has the highest degree of perpendicular local ordering within the first coordination shell. Perpendicular arrangements among neighboring molecules are progressively lost as one goes from Bz to HFB and TFB. However, the average difference between the two extreme situations is given only by 5% in $N_1^{\parallel}$ and $N_1^{\perp}$. This seems to be enough to yield such different characteristics in the local structure of TFB, as observed in Figures 1 and 2.

B. Local Intermolecular Dynamics. The translational and rotational dynamics in liquids can be analyzed in terms of autocorrelation functions of the molecular center of mass and angular velocities. The study of velocity TCFs can be extended to momentum transfer and intermolecular velocity correlations[63−67] by investigating the correlations between motions of distinct

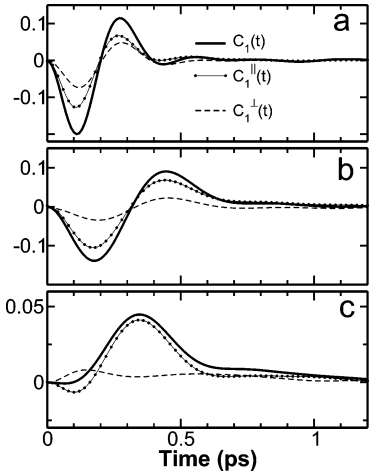

Figure 4. Angular velocity CCFs within the first coordination shell, $C_1(t)$, and contributions to them from parallel $[C_1^{\parallel}(t)]$ and perpendicular arrangements $[C_1^{\perp}(t)]$ for (a) Bz, (b) HFB, and (c) TFB.

molecules. Velocity cross-correlation functions (CCFs) between neighboring molecules can be computed from[68−70]

$$C_n(t) = \frac{\langle \boldsymbol{v}_i(0)\cdot\boldsymbol{v}_j(t)\rangle_n}{\langle v_i^2\rangle} \tag{22}$$

where $\boldsymbol{v}_i$ represents either the linear center-of-mass velocity or $\boldsymbol{\omega}_i$, the angular velocity of molecule i; and $\langle ...\rangle_n$ is a restricted statistical average correlating the velocity of molecule i with molecules in its nth coordination shell, corresponding to the initial intermolecular separations in the range $d_n \le r \le D_n$

$$\langle \boldsymbol{v}_i(0)\cdot\boldsymbol{v}_j(t)\rangle_n = \frac{1}{N_n}\langle \boldsymbol{v}_i(0)\cdot\sum_j \boldsymbol{v}_j(t)F_n(r_{ij})\rangle \tag{23}$$

N_n is the number of neighbors within the nth coordination shell, and $F_n(r)$ in the above equation represents a function that selects from the summation the pairs whose intermolecular distance at $t = 0$ lies within the desired range

$$F_n(r) = \Theta(r(0) - d_n)\,\Theta(D_n - r(0)) \tag{24}$$

with $\Theta(r)$ the Heaviside step function and $r(0)$ representing the initial distance between the centers of mass of molecules i and j in the nth shell.

The analysis of velocity CCFs is performed over different coordination shells because, as pointed out already by Endo and Endo,[65] the details of molecular motions revealed by these microscopic velocity CCFs would be averaged out and remain hidden if the correlation functions for the whole system were used. Furthermore, if we want a more detailed picture revealing how the transfer of momentum takes place among molecules with parallel or perpendicular ordering, it is possible to isolate the contributions $C_1^{\parallel}(t)$ and $C_1^{\perp}(t)$ out of $C_1(t)$ by simply including the factor $F_n(\theta_{ij})$ inside the average of eq 23. $F_n(\theta)$ will select from the summation the pairs for which the initial angle θ between symmetry axes lies in the range $\theta_{min} \le \theta \le \theta_{max}$. We keep the same convention for $C_1^{\parallel}(t)$ and $C_1^{\perp}(t)$ as for $N_1^{\parallel}$ and $N_1^{\perp}$, corresponding to $0 \le \theta \le \pi/4$ and $\pi/4 \le \theta \le \pi/2$, respectively.

Figure 4 displays the angular velocity CCFs within the first coordination shell for the three liquids, along with their components arising from parallel and perpendicular arrangements. The value of d_1 was set to zero, and the values of D_1

were taken from the location of the first minimum of $g_{cm}(r)$ (see Figure 2), and can be found in Table 3.

An extensive analysis of angular velocity CCFs in liquid Bz and HFB can be found in ref 5. We focus here on the main differences found for the three liquids. At short time delays, $C_1(t)$ for Bz and HFB is negative, implying that the transfer of angular momentum from the tagged central molecule to neighboring molecules occurs initially because of rotations in opposite directions. The simplified picture of a pair of coupled gears is usually used to illustrate this situation.[67] This statement also holds true for the cross correlations among parallel and perpendicular pairs of molecules in Bz and HFB, exhibiting $C_1^{\parallel}(t)$ and $C_1^{\perp}(t)$ their maximum and minimum peaks at roughly the same locations for each liquid, with somewhat higher intensities corresponding to the parallel peaks.

However, in TFB, the maxima in $C_1(t)$ and $C_1^{\parallel}(t)$ have a much larger amplitude than the corresponding minima; and more interestingly, $C_1^{\perp}(t)$ is positive at short times, opposite to the behavior in Bz and HFB. This finding indicates that in TFB the transfer of angular momentum in the first shell occurs initially through rotations in opposite directions for parallel structures, while there are rotations in the same direction as the central tagged molecule for perpendicular arrangements.

The above behavior can be explained by inspecting some snapshots of the MD trajectory, focusing on the joint dynamics of three neighboring molecules, as shown in Figure 5. Molecules labeled as M2 and M3 in Figure 5 are both within the spherical first shell around molecule M1. Thus, because of the strong parallel local order, while the angles between M1 and M2 and between M2 and M3 are both smaller than 45°, there will be some instances for which the angle between molecules M1 and M3 is greater than 45°, so this pair will be classified as belonging to the perpendicular group. The molecules will exhibit librational motions at short times; Figure 4c indicates that these fast rotations occur in opposite directions between parallel molecules such as molecules M1 and M2, as reflected in the negative sign of $C_1^{\parallel}(t)$ at short times, and the same situation could be happening between molecules M2 and M3. As a result, it is likely that the librational motions between perpendicular molecules M1 and M3 occur in phase, or, in other words, their rotations occur in the same direction.

Of course, the above scenario is not the only possible way of accounting for the behavior of $C_1(t)$ and its components in TFB. Additional information on angular velocity cross-correlations would be needed to determine the actual mechanism. For example, because M3 is likely to move into the second coordination shell of M1 from the first one, extending the analysis to additional coordination shells might provide useful information. However, such a detailed study of orientational cross-correlations is beyond the scope of this work.

V. Polarizability Anisotropy Relaxation

Now we discuss our results for the polarizability anisotropy relaxation in the three liquids studied, using the site−site DID model for $\mathbf{\Pi}^{\mathrm{I}}$.

The result of the projection scheme for the polarizability anisotropy relaxation in Bz can be seen by comparing Figure 6a to Figure 6b, where the unprojected and projected components of the polarizability anisotropy TCF are displayed. Figure 6b shows reorientational and CI polarizability correlations, $\psi_{xz}^{\mathrm{R}}(t)$ and $\psi_{xz}^{\mathrm{CI}}(t)$, and their R−CI cross-correlation, $\psi_{xz}^{\mathrm{Cross}}(t)$.

The intensities of $\psi_{xz}^{\mathrm{CI}}(t)$ and $\psi_{xz}^{\mathrm{Cross}}(t)$ are small compared to that of $\psi_{xz}^{\mathrm{R}}(t)$; at times beyond ∼7 ps CI and Cross contributions have already died out, and $\psi_{xz}^{\mathrm{R}}(t)$ is clearly the dominant contribution to $\psi_{xz}(t)$. Therefore, on this time scale the main effect of interaction-induced contributions is to modify the intensity of the collective reorientational component through the local-field factor $(1 + f_{xz})^2$.

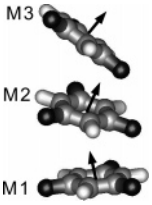

Figure 5. Typical snapshot of three 1,3,5-trifluorobenzene molecules (labeled as M1, M2, and M3, see text) during the MD simulation. The arrows indicate the direction of the symmetry axis.

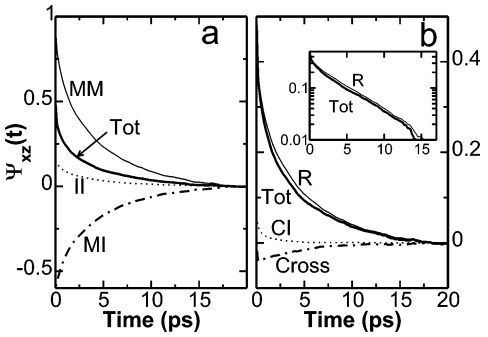

Figure 6. Contributions to the total polarizability anisotropy TCF from (a) unprojected and (b) projected polarizability components, for liquid benzene. The inset in panel b shows the decay of the reorientational component and total TCF on semilog scale. Note the different scales of the *y* axis in panels a and b.

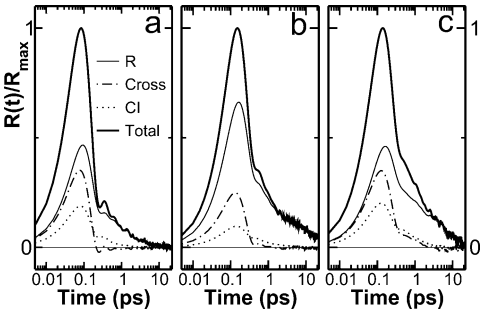

Figure 7. Contributions to the total nuclear response function $R(t)$ from projected reorientational (R), collision-induced (CI) polarizability anisotropy components, and the cross term between them, for (a) Bz, (b) HFB, and (c) TFB.

Figure 7 shows the projected components of the nuclear response function, $R(t)$, for the three liquids. For Bz and HFB the reorientational contribution is dominant after ∼0.3 ps, but in TFB it takes a bit longer for reorientations to dominate the nuclear response, requiring times of the order of 2−3 ps. In all three liquids, the maximum intensity of the cross R−CI component is larger than that of CI contribution.

A. Local Pair Contributions to $\psi_{xz}^{\mathrm{MM}}(t)$. We shall now focus on the study of the molecular contribution, $\psi_{xz}^{\mathrm{MM}}(t)$, to the total polarizability anisotropy TCF in order to determine how it is affected by the local structure and dynamic pair correlations. $\psi_{xz}^{\mathrm{MM}}(t)$ is given by

$$\psi_{xz}^{\mathrm{MM}}(t) = \frac{1}{\Gamma^2}\langle \Pi_{xz}^{\mathrm{M}}(0)\, \Pi_{xz}^{\mathrm{M}}(t)\rangle \qquad (25)$$

Recalling that Π_{xz}^{M} is given by eq 5, and the fact that for axially

TABLE 4: Static Second-Rank Orientational Factor (g_2) and Parameters Obtained from the Fitting of the Normalized Functions $\bar{\psi}_1^{\dagger}(t)$ to Single Exponential Functions $f(t) = A \exp(-t/\tau_1^{\dagger})$

liquid	g_2	$\tau_1^{\parallel}$/ps	$\tau_1^{\perp}$/ps	$\tau_1^{\parallel}/\tau_1^{\perp}$
Bz	0.92	4.10	3.72	1.10
HFB	1.51	14.83	11.89	1.25
TFB	1.91	6.47	4.62	1.40

symmetric molecules the isolated-molecule polarizability tensors in the laboratory frame are given by eq 8, $\psi_{xz}^{\mathrm{MM}}(t)$ can similarly be written in terms of the second-order Legendre polynomial, $P_2(x) = (3x^2 - 1)/2$, as[23]

$$\psi_{xz}^{\mathrm{MM}}(t) = \frac{1}{N}\sum_{i,j}^{N} \langle P_2[\hat{\mathbf{u}}_i(0)\cdot\hat{\mathbf{u}}_j(t)]\rangle \tag{26}$$

$\psi_{xz}^{\mathrm{MM}}(t)$ can also be separated into single-molecule and pair contributions

$$\psi_{xz}^{\mathrm{MM}}(t) = \psi_{xz}^{\mathrm{MMs}}(t) + \psi_{xz}^{\mathrm{MMp}}(t) \tag{27}$$

where $\psi_{xz}^{\mathrm{MMs}}(t)$ is the single-molecule component, arising from terms with $i = j$, and $\psi_{xz}^{\mathrm{MMp}}(t)$ is the pair (or distinct) contribution obtained from the remaining terms ($i \neq j$) in the summation of eq 26. Note that $\psi_{xz}^{\mathrm{MMs}}(0) = 1$ by definition, and thus $\psi_{xz}^{\mathrm{MMp}}(0)$ modifies the initial unity value with a contribution from static orientational pair correlations.

The static second rank orientational pair correlation factor for molecular anisotropic polarizability components is defined as the initial value of the molecular TCF[20,71,24]

$$g_2 = \langle(\Pi_{xz}^{\mathrm{M}})^2\rangle/\Gamma^2 = \psi_{xz}^{\mathrm{MM}}(0) \tag{28}$$

In the absence of orientational pair correlations, $g_2 = 1$ (see eqs 26−27); the greater the tendency for local parallel or antiparallel ordering, the larger the value of $\langle P_2[\hat{\mathbf{u}}_i\cdot\hat{\mathbf{u}}_j]\rangle$ for $i \neq j$, and thereby, of g_2. In the rotational-diffusion limit, the single-molecule orientational TCF for symmetric top molecules decays exponentially, characterized by a relaxation time τ_s, and the collective orientational function is also exponential with a relaxation time τ_c; these times are related by[16]

$$\tau_c = \left(\frac{g_2}{j_2}\right)\tau_s \tag{29}$$

where j_2 is a dynamic orientational correlation parameter. In much of the literature, j_2 is assumed to be equal to unity,[72,24,73] and as a consequence, $g_2 \approx \tau_c/\tau_s$. We have tested the degree of accuracy of this approximation in liquid acetonitrile and chloroform,[25] at room temperature, obtaining values for j_2 close to unity with more than 99% accuracy. However, in previous work[47] we obtained a value of $j_2 \approx 0.7$ for Bz and HFB. The experimental estimation in these liquids, performed by Bauer et al.[74] from depolarized Rayleigh scattering and NMR relaxation, yielded dynamical correlation factors of $j_2 = 0.8$ and 1.06 for Bz and HFB, respectively. The static correlation factors reported in that work[74] are $g_2 = 0.8$ for Bz and $g_2 = 1.40$ for HFB, in close agreement with our computed values (see Table 4). Therefore, as discussed in ref 47, we believe that the poor agreement between theory and experiments for the estimation of j_2 in HFB is probably due to an overestimation of the intermolecular interactions in the model potential, which predicts a collective relaxation time, τ_c, much longer than that obtained from experiments.[47]

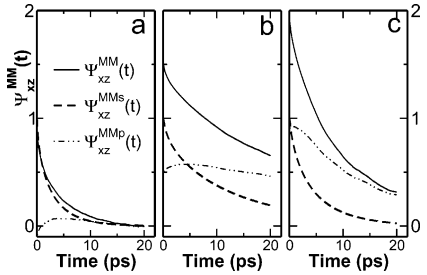

Figure 8. Single (− − −) and pair (− · · −) contributions to the total molecular polarizability anisotropy TCF, $\psi_{xz}^{\mathrm{MM}}(t)$ (solid line), for (a) Bz, (b) HFB, and (c) TFB.

Experimental values reported for g_2 of Bz lie in the range of 0.78−1.16, whereas for HFB the reported range for g_2 is wider, 1.4−2.75, (refs 72 and 74−78) and for TFB the experimental value is close to 2 (ref 39). Our computed values for g_2, shown in Table 4, lie within the range of experimental data, and the increase in g_2 from Bz to HBF and TFB is consistent with the greater extent of parallel local ordering in these liquids.

Figure 8 shows the single, pair, and total molecular TCFs for the three liquids. We note that in all three liquids $\psi_{xz}^{\mathrm{MMp}}(t)$ exhibits a very slow decay rate in the time scale shown in Figure 8, especially for Bz and HFB, and has a lower intensity than $\psi_{xz}^{\mathrm{MMs}}(t)$ at short times. It is possible that the total $\psi_{xz}^{\mathrm{MMp}}(t)$, which represents an average over all pairs, including weakly correlated distant ones, is obscuring the details of orientational correlations among near neighbors. Hence, we could define a local pair correlation function by averaging the orientational quantity P_2 only over pairs of molecules that have an initial intermolecular separation within a distance range of the nth coordination shell, $d_n \leq r \leq D_n$ (we omit the subscript xz in the TCF for simplicity)

$$\psi_n^{\mathrm{MMp}}(t) = \frac{1}{N}\sum_{i,j}^{N}{}' \langle P_2[\hat{\mathbf{u}}_i(0)\cdot\hat{\mathbf{u}}_j(t)]F_n(r_{ij})\rangle \tag{30}$$

where $F_n(r)$ has been defined previously in eq 24. The primed summation in eq 30 means that the terms $i = j$ are excluded. The average $\langle ... \rangle$ is then an ordinary statistical average over molecular pairs and time origins.

Moreover, to get a more detailed picture of how rapidly or slowly different characteristic arrangements of distinct molecules in the nth shell decorrelate with time, it is possible to isolate contributions to $\psi_n^{\mathrm{MMp}}(t)$, within a given initial range of relative orientations θ_{ij}, defined as, $\theta_{ij}(0) = \cos^{-1}(|\hat{\mathbf{u}}_i\cdot\hat{\mathbf{u}}_j|)$ by including the factor $F_n(\theta_{ij})$ inside the average of eq 30

$$\psi_n^{\theta}(t) = \frac{1}{N}\sum_{i,j}^{N}{}' \langle P_2[\hat{\mathbf{u}}_i(0)\cdot\hat{\mathbf{u}}_j(t)]F_n(r_{ij})\, F_n(\theta_{ij})\rangle \tag{31}$$

The same two angular ranges as in Section IV.B have been considered here for pairs of molecules within the first shell, that is, $0 \leq \theta < \pi/4$ and $\pi/4 \leq \theta \leq \pi/2$; and using the same notation as before, we will denote the corresponding TCF pair contributions by $\psi_1^{\parallel}(t)$ and $\psi_1^{\perp}(t)$, respectively. The components of $\psi_{xz}^{\mathrm{MMp}}(t)$ are displayed in Figure 9.

It can be seen that the rapidly decaying portion of $\psi_1^{\parallel}(t)$ is to a large extent canceled by that of $\psi_1^{\perp}(t)$, of opposite sign, leaving as a result, in the case of Bz and HFB, a very slowly decaying pair correlation function $\psi_1^{\mathrm{MMp}}(t)$. The extent of

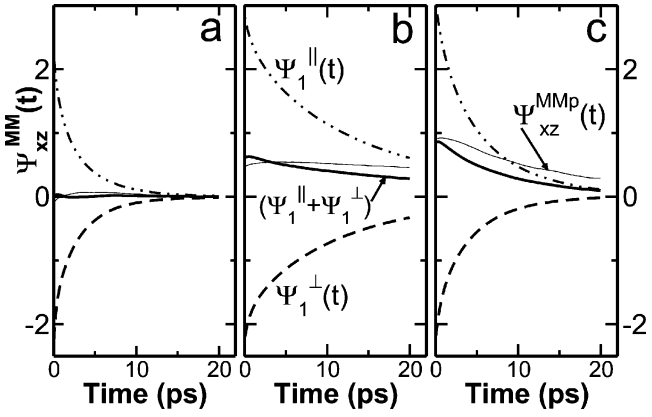

Figure 9. Contributions $\psi_1^{\parallel}(t)$ (− · · −) and $\psi_1^{\perp}(t)$ (− − −), the sum of these two (bold solid line), and the total pair contribution, $\psi_{xz}^{MMp}(t)$ (thin solid line), for (a) Bz, (b) HFB, and (c) TFB.

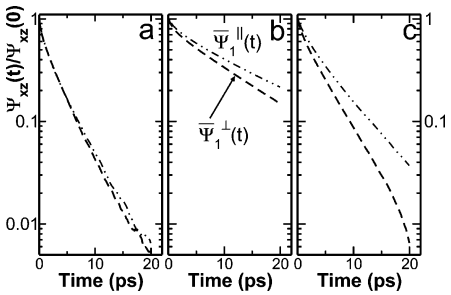

Figure 10. Normalized contributions $\bar{\psi}_1^{\parallel}(t)$ (− · · −) and $\bar{\psi}_1^{\perp}(t)$ (− − −), for (a) Bz, (b) HFB, and (c) TFB, on a semilog scale.

cancellation of the rapidly decaying portion of $\psi_1^{MMp}(t)$ diminishes as the average number of neighbors arranged in parallel configurations within the first coordination shell increases, which happens in going from Bz to TFB. The initial values of $\psi_1^{\parallel}(t)$ and $\psi_1^{\perp}(t)$ provide information about the average relative orientations of molecules in the first shell. Namely, using the values of $\psi_1^{\parallel}(0)$ and $N_1^{\parallel}$, we estimate the average angle between symmetry axes of neighboring molecules to be 30.9, 29.9, and 29.2° for Bz, HFB, and TFB, respectively; a similar analysis considering $\psi_1^{\perp}(0)$ and $N_1^{\perp}$ yields 65.9, 65.6, and 65.8° for the same fluids.

A comparison of the decay rates of $\psi_1^{\parallel}(t)$ and $\psi_1^{\perp}(t)$ might be done by normalizing these functions, $\bar{\psi}_1^{\dagger}(t) = \psi_1^{\dagger}(t)/\psi_1^{\dagger}(0)$, where † represents either ∥ or ⊥. These normalized functions are plotted on a semilog scale in Figure 10. Although the difference in the decay rates is almost negligible in benzene, substantially slower decay rates for $\bar{\psi}_1^{\parallel}(t)$ than for $\bar{\psi}_1^{\perp}(t)$ are found for HFB and TFB. These functions can be well fitted by single exponentials at long times. The fit parameters are shown in Table 4.

We observe in Figure 10 that the diffusive dynamics of molecules arranged initially in parallel configurations, within the first coordination shell, are more hindered than for perpendicular structures, the former always decaying more slowly. The ratio between parallel and perpendicular diffusive decay times, $(\tau_1^{\parallel}/\tau_1^{\perp})$, shown in Table 4, is largest for TFB.

B. OKE Spectra. We analyze in the frequency domain the OKE spectra obtained by Fourier−Laplace transforming the nuclear response function $R(t)$, using eq 4. The OKE spectra are displayed in Figure 11. Panel a shows the total OKE spectra and panel b, the reduced OKE (ROKE) susceptibilities, computed by subtracting the diffusive orientational contribution to $R(t)$ in the usual way.[38,39,79] In previous work,[47] we found good

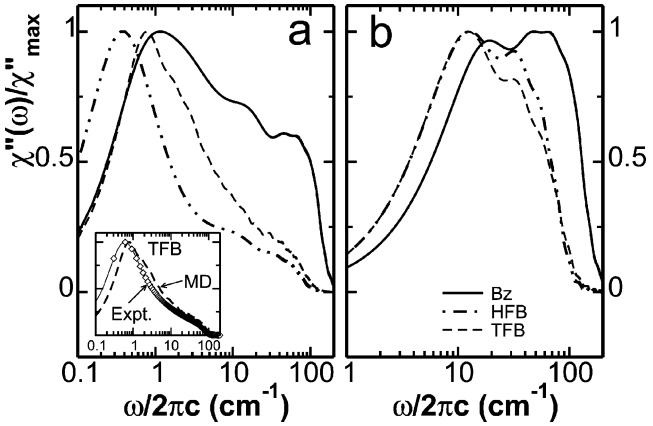

Figure 11. Normalized OKE spectral density (a) and reduced spectral density (b) for liquid Bz (−), HFB (− · · −), and TFB (− − −). The inset in panel a shows the comparison between the experimental (provided by J. T. Fourkas, ref 39) and the computed OKE spectra for TFB.

agreement between the computed OKE spectra and experimental data on Bz and HFB[38,39,80] using the same model for the interaction-induced polarizability as in the present work. The inset in Figure 11a, in which the computed and the experimental OKE spectra for TFB are displayed, shows that the agreement between theory and experiments is also good for TFB.

Loughnane et al.[39] proposed a model that relates the shapes of the ROKE spectra with the local structure, in which they assume that the librational frequencies depend on local arrangements among neighboring molecules. Because the ROKE spectrum of Bz has the greatest intensity in the high-frequency region, and is also the liquid, in this set, with the greatest degree of perpendicular order, the authors assume, accordingly, that perpendicular structures have higher librational frequencies than parallel ones. They justify this assignment in terms of the differences between the crystal structure and the local structure found in the liquid phase. Namely, the crystal structures of Bz and HFB consist of a herringbone pattern in which the molecules are locally arranged roughly perpendicular to each other,[81] whereas the nonnegligible degree of parallel ordering found in the liquid phase in Bz and HFB would result in inefficient packing, and therefore, in lower librational frequencies.

To test this model, we calculated the local contribution to the librational spectrum as follows. First, we computed the local MM TCFs by considering the molecules that are initially and at time t within the first coordination shell, and participating at both times in parallel or perpendicular structures. This was done by using eq 31 without the restriction $i \neq j$ (and then considering both pair and single-molecule contributions) and including in addition the factors $\Theta(D_1 - r_{ij}(t))$, $\Theta(\pi/4 - \theta_{ij}(t))$ (or the factor corresponding to perpendicular arrangements) inside the average. From the local functions $\psi_1^{MM,\parallel}(t)$ and $\psi_1^{MM,\perp}(t)$, the corresponding nuclear response functions were derived. Second, the diffusive contributions to these functions was subtracted in the usual way,[39,38,79] and the ROKE local spectra were obtained by performing a Fourier−Laplace transform. These ROKE spectra arising from local MM correlations are displayed in Figure 12. By comparing the ROKE spectra arising from MM contributions in the first shell, displayed in Figure 12 with solid lines, to the total ROKE spectra of Figure 11b, we see that the second peaks present in the latter spectra at ∼60 cm^{-1} in Bz and around 20−30 cm^{-1} in HFB and TFB are absent from the ROKE spectra $\chi''_{MM}(\omega)$, making the total ROKE spectra look broader, especially for Bz. The total ROKE spectrum contains contributions not only from nondiffusive orientational modes but also from

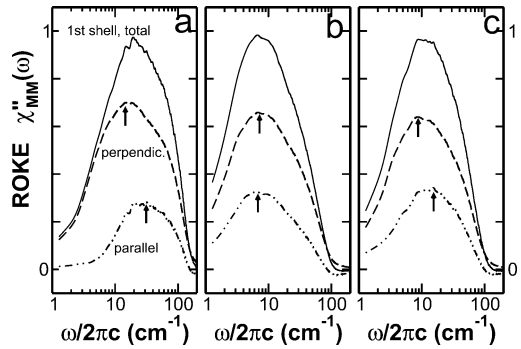

Figure 12. Normalized ROKE spectral densities arising from MM correlations, for molecules participating in parallel (− ·· −) or perpendicular (− − −) arrangements within the first coordination shell, for (a) Bz, (b) HFB, and (c) TFB, on a semilog scale. The arrows indicate the position of the maxima. The total MM spectra within the first shell (solid lines) are normalized with their maximum value.

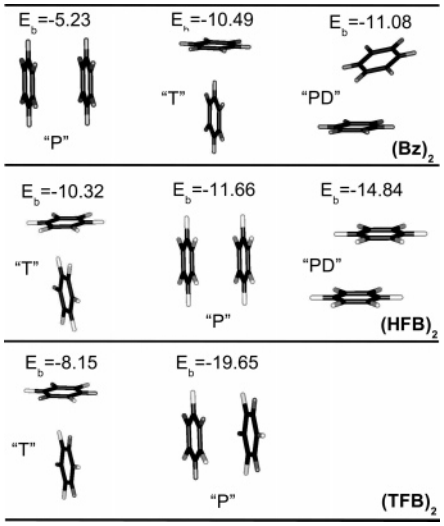

Figure 13. Minimum energy structures for Bz (top), HFB (middle), and TFB (bottom) dimers. The binding energy (E_b) is written in kJ/mol. Labels P, T, and PD refer to parallel, T-shaped (perpendicular), and parallel-displaced geometries, respectively.

translations and cross translational-orientational modes, whereas the reduced spectrum $\chi''_{MM}(\omega)$ is only due to nondiffusive molecular reorientations. Hence, we assign the contributions in the high-frequency portion of the ROKE spectra to those nonorientational dynamical modes not considered in $\chi''_{MM}(\omega)$. Indeed, the projected parts of the OKE spectrum, $\chi''_{CI}(\omega)$ and $\chi''_{Cross}(\omega)$ (to be shown in Figure 15) contribute predominantly in the high-frequency region of the spectrum, as found also for other liquids such as acetonitrile and chloroform.[25]

We observe in Figure 12, that for Bz and TFB the parallel contribution to the ROKE librational spectrum is slightly shifted toward higher frequencies with respect to the perpendicular band, whereas in HFB the maxima of parallel and perpendicular bands are roughly coincident. At first glance this seems surprising, because the local structures found in Bz and TFB are quite different. However, an inspection of the binding energies corresponding to the optimized dimer structures may help explain the features shown in Figure 12.

Figure 13 displays the minimum energy structures and the associated binding energies, computed using the Williams potential model, for Bz, HFB, and TFB dimers, labeled as P (parallel), T (T-shaped or perpendicular), and PD (parallel displaced) depending on their geometry. In previous work,[47] we found three local minima for Bz and HFB dimers, with the

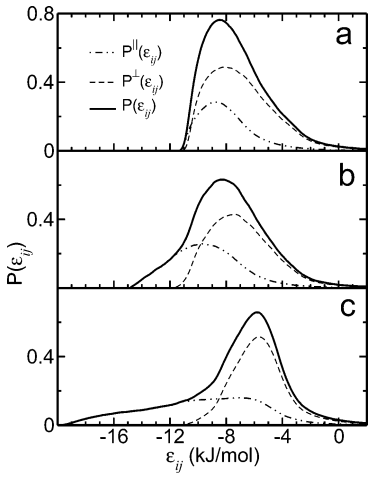

Figure 14. Pair energy probability distributions, $P(\varepsilon_{ij})$, considering only the closest four neighbors, separated into parallel and perpendicular configurations, for (a) Bz, (b) HFB, and (c) TFB. The area under the total curve $P(\varepsilon_{ij})$ is normalized to four.

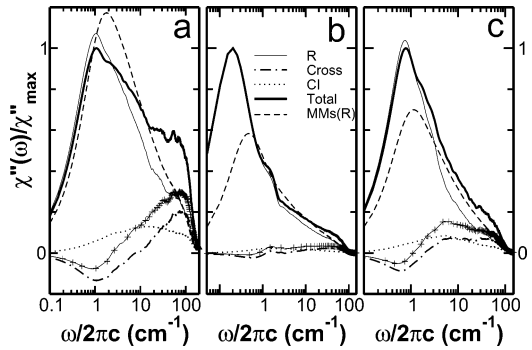

Figure 15. Projected contributions to normalized OKE spectral density for (a) liquid Bz, (b) HFB, and (c) TFB, on a semilog scale. The single-molecule contribution to the projected reorientational polarizability anisotropy TCF is also shown [MMs(R)], normalized with χ''_{max}.

global minimum binding energies corresponding to PD configurations. In the Bz dimer, the molecular planes in the PD geometry are not exactly parallel, but they form an angle of ∼25° and this structure belongs to the parallel classification in our scheme, where the limiting angle dividing between parallel and perpendicular arrangements was taken as 45°. The binding energy at the T minimum in $(Bz)_2$ lies very close to that of the PD minimum, just 0.59 kJ/mol above it. The first two minima in HFB dimers are close in energy, whereas the E_b at the global minimum, in PD geometry, lies ∼4 kJ/mol below them. In TFB dimers, only two minimum structures were found, corresponding to T and P geometries. The P structure is the global minimum and the T structure is separated from it by 11.5 kJ/mol. Note that in this last case the molecules are in a face-to-face configuration but their planes are rotated by 30° with respect to each other.

In the liquid phase, all of these dimer arrangements are competitive, and the resulting average numbers of neighbors arranged in parallel and perpendicular configurations within the first coordination shell are displayed in Table 3 of Section IV.A. Now, in view of the analysis of the minimum energy structures in dimers, it is reasonable to expect higher librational frequencies for parallel structures than for perpendicular arrangements in this set of liquids, because the intermolecular potential energy becomes stiffer for parallel arrangements at short separations.

Because in the liquid phase the intermolecular interactions between pairs (ε_{ij}) are not necessarily identical to the binding energies calculated for isolated dimers, we computed the

probability distribution function of pair energies, $P(\varepsilon_{ij})$, displayed in Figure 14. In the analysis of $P(\varepsilon_{ij})$, we considered only the nearest four neighbors of a given molecule (out of the 12−13 that lie within the first spherical shell). We have chosen to consider only the closest four neighbors in the analysis of $P(\varepsilon_{ij})$ based on the crystal structure found for Bz. In the crystalline phase, each Bz molecule has a first coordination shell made of four molecules at a distance of 5.08 Å, oriented perpendicularly to the central one, and a second coordination shell of four molecules at 5.9 Å with parallel orientation, plus four additional molecules at 6.05 Å, again with perpendicular orientation relative to the central one,[6] making an effective second shell out of a total of eight molecules.

We see that the maximum of $P^{\parallel}(\varepsilon_{ij})$, the contribution from parallel orientations, is located always at lower pair energies than the maximum of $P^{\perp}(\varepsilon_{ij})$. The correlation between Figures 12 and 14 is clear for TFB. Among the closest four neighbors of a given molecule, parallel arrangements reach the lowest intermolecular energies, with a probability distribution $P^{\parallel}(\varepsilon_{ij})$ that extends well beyond lower values of ε_{ij} than $P^{\perp}(\varepsilon_{ij})$. Parallel arrangements exhibit then the highest librational frequencies in Figure 12c.

In HFB, the difference in the location of the maxima of $P^{\parallel}(\varepsilon_{ij})$ and $P^{\perp}(\varepsilon_{ij})$ is $\Delta\varepsilon_{ij} \approx 3$ kJ/mol, very similar to the difference found for the binding energies (ΔE_b) of the isolated dimers P (or PD) and T. Compared to TFB, both $\Delta\varepsilon_{ij}$ and ΔE_b for P and T dimers are smaller in HFB, and, in addition, the moment of inertia for tumbling motions is roughly twice as large as that of TFB. Consequently, the difference in the location of parallel and perpendicular librational bands of the ROKE spectrum is smaller in HFB than in TFB.

In the case of Bz, the ΔE_b value between PD and T dimers is roughly 0.6 kJ/mol, even smaller than in HFB, so it is surprising to observe a noticeable shift in the librational bands in Figure 12a. However, the difference $\Delta\varepsilon_{ij}$ in Figure 14a is roughly twice the value found for ΔE_b in the isolated dimers. We presume that this small stabilizing effect of the liquid phase on parallel structures relative to perpendicular arrangements at short distances, as compared to isolated dimers, could explain the shift of the parallel librational band toward higher frequencies in Bz.

It is also worth mentioning that the relative locations of the maxima of $P(\varepsilon_{ij})$ for the next closest eight neighbors (not shown) follow a trend opposite of that observed for the closest four molecules. Namely, in this case the maximum of $P^{\perp}(\varepsilon_{ij})$ always occurs at lower energies than $P^{\parallel}(\varepsilon_{ij})$. Therefore, considering the link found between pair energy distributions and the librational molecular spectra for parallel and perpendicular arrangements of neighboring molecules, the effect seen in Figure 12, in which all the molecules inside the first coordination sphere were considered, seems to arise mainly from the closest four neighbors inside the first coordination shell. The shift observed in Figure 12 is also more likely to be related to a harmonic librational oscillator model, for which the modes with strongest intermolecular interactions have higher librational frequencies, than to relative orientations that result in less efficient packing than in the crystal.

The projected contributions to the total OKE susceptibility are depicted in Figure 15, along with the single-molecule molecular susceptibility. At low frequencies, there is a huge contribution from the reorientational component, having a maximum at about 1, 0.2, and 0.8 cm^{-1} for Bz, HFB, and TFB, respectively. In the same panels, we have plotted the contribution to the reorientational susceptibility, χ''_R, originating from the single-molecule TCF, $[\psi_{xz}^{MMs(R)}(t) = (1 + f_{xz})^2\psi_{xz}^{MMs}(t)]$, also normalized with χ''_{max}. The single-molecule orientational component, MMs(R), makes an important contribution in the low-frequency region, exhibiting a sharp peak at around 0.5−1.5 cm^{-1}. We note also that the total and reorientational curves are roughly coincident at very low frequencies; in fact, these contributions are known to arise from the slow orientational diffusive relaxation. The higher-frequency portion of the spectrum has its origin in intermolecular vibrational motions, a region in which the nonorientational components, that is, the collision-induced and cross components, make the main positive contribution to $\chi''(\omega)$, especially in Bz, as displayed in Figure 15 by the lines with "+" symbols.

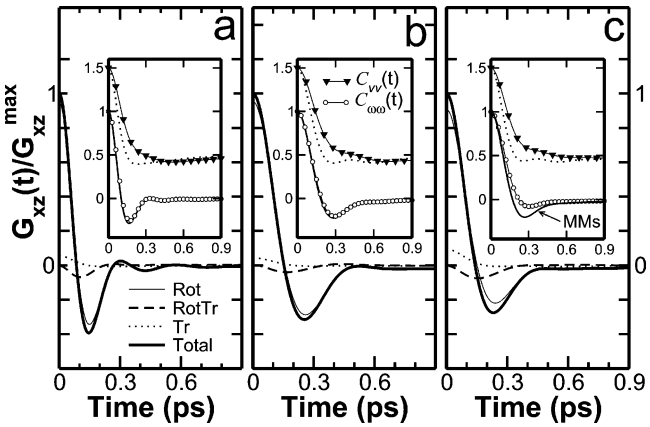

Figure 16. Normalized contributions to the polarizability velocity TCF, $G_{xz}(t)/G_{xz}^{max}$, from rotational (Rot), translational (Tr), and the rotation-translational coupling (RotTr) components for (a) Bz, (b) HFB, and (c) TFB. The insets show a comparison between the polarizability velocity TCF arising from single-molecule correlations (MMs, solid line) and $C_{\omega\omega}(t)$ (circles); and between $G_{xz}^{Tr}(t)$ and $C_{vv}(t)$ (triangles). The latter two curves are shifted vertically by +0.5 for clarity.

C. Polarizability Velocity TCFs. As discussed already in Section II.B., Steele theory provides an alternate way of analyzing the dynamical origin of polarizability relaxation. In this approach, the starting point is $G_{xz}(t)$ (see eq 14), the TCF of the collective polarizability anisotropy velocity.

Figure 16 shows the different contributions to the normalized polarizability anisotropy velocity TCF, $G_{xz}(t)/G_{xz}^{max}$, using eq 15. At first glance, by comparing the relaxation times of $G_{xz}(t)$ in Figure 16a to those of the polarizability anisotropy TCF, $\psi_{xz}(t)$, in Figure 6, it is evident that although the latter correlations need about 15 ps to decay to zero, the correlations in $G_{xz}(t)$ decay much faster, that is, the oscillations observed in Figure 16 have practically already died out after 1 ps or less. All of the $G_{xz}(t)$ components in Figure 16 change sign and exhibit local extrema. A common feature that is evident in the three liquids is the large contribution that the rotational term $G_{xz}^{Rot}(t)$ makes to $G_{xz}(t)$ over the whole time scale. The zero time amplitude of $G_{xz}(t)$ is proportional to the spectral second moment measured in frequency-domain depolarized light scattering experiments, and by breaking it up into its Rot, Tr, and RotTr components (or, alternatively, into its MM, MI, and II contributions), it allows us to determine which variables give important contributions to this quantity. The initial values of $G_{xz}(t)/G_{xz}^{max}$ are listed in Table 5.

For the three liquids, the initial amplitude of $G_{xz}(t)$ is largely given by rotational degrees of freedom. However, it can be seen that although the relative rotational contribution is roughly similar for Bz, HFB, and TFB, for the latter fluid the translational component is about twice as large as that in Bz and HFB.

TABLE 5: Zero Time Amplitude Components of $G_{xz}(t)/G_{xz}^{max}$

component	Bz	HFB	TFB
Rot	0.947	0.953	0.908
RotTr	−0.002	0.003	−0.001
Tr	0.055	0.044	0.094
MM	0.913	0.929	0.898
MI	−0.039	−0.017	−0.061
II	0.126	0.088	0.163
II, Rot	0.055	0.044	0.070
II, Tr	0.071	0.044	0.093
II, RotTr	0.000	0.000	0.000

Figure 16 displays in the insets a comparison between the autocorrelation function of the center-of-mass angular (tumbling) velocity, $C_{\omega\omega}(t) = \langle \boldsymbol{\omega}_i^t(0)\cdot\boldsymbol{\omega}_i^t(t)\rangle$ and the single-molecule polarizability velocity TCF, $G_{xz}^{MMs}(t)$, which is defined, by analogy with $\psi_{xz}^{MMs}(t)$, as

$$G_{xz}^{MMs}(t) = \frac{1}{\Gamma^2}\sum_{i=1}^{N}\langle \dot{\alpha}_{xz,i}(0)\,\dot{\alpha}_{xz,i}(t)\rangle \tag{32}$$

and therefore, contains products of angular velocities and orientational coordinates (see eqs A.1−A.2). Because spinning motions are not relevant to OKE, because they cannot change the polarizability, only $\boldsymbol{\omega}_i^t(t)$, the component of the angular velocity for reorientation of the molecular plane, that is, the tumbling angular velocity, is considered in the computation of $C_{\omega\omega}(t)$.

If the velocity part of $G_{xz}^{MMs}(t)$ decays rapidly compared to changes in the coordinates, one would expect that its decay would be similar to that for the tumbling velocity autocorrelation, $C_{\omega\omega}(t)$.[28] This is indeed what we find for Bz and HFB, as can be seen from the insets in Figure 16. In the case of TFB, however, $G_{xz}^{MMs}(t)$ exhibits a deeper minimum than the tumbling velocity autocorrelation, revealing that the correlations arising from the orientational coordinates make an additional contribution to the decay rate of $G_{xz}^{MMs}(t)$, especially at short times.

The comparison between the normalized translational polarizability correlations, $G_{xz}^{Tr}(t)$, and the autocorrelations of the linear center-of-mass velocity, $C_{vv}^{TR}(t) = \langle \boldsymbol{v}_i(0)\cdot\boldsymbol{v}_i(t)\rangle$, is also displayed in the insets of Figure 16. Roughly speaking, $G_{xz}^{Tr}(t)$ can be thought of as a product between the correlations of a generalized force (defined as the derivative of the collective polarizability with respect to translational coordinates) and the correlations of the linear center-of-mass velocities. Again, if the changes in the generalized forces are slow compared to those of the linear velocities, $G_{xz}^{Tr}(t)$ should decay in a way similar to $C_{vv}(t)$. However, it can be observed that $G_{xz}^{Tr}(t)$ relaxes at a noticeably faster rate than $C_{vv}(t)$ does at short times for the three liquids, indicating that the correlations of the generalized forces contribute on the same time scale as the center-of-mass velocity correlations, enhancing the decay rate of $G_{xz}^{Tr}(t)$.

In view of the fact that the interaction-induced polarizability velocity, given by eq A.3, has rotational and translational components, it might be interesting to investigate how much of the interaction-induced polarizability velocity TCF, $G_{xz}^{II}(t)$, is due to rotational, translational, and rotational-translational correlations. The initial intensities of these contributions to $G_{xz}^{II}(0)$ are also reported in Table 5.

The zero-time intensities can be understood as the corresponding equilibrium averages in which coordinates and velocities are canonical independent variables. As a consequence, any polarizability velocity TCF containing an odd power of any translational or orientational velocity component must vanish.[28] Because $G_{xz}^{RotTr}(0)$ contains correlations between angular and linear velocities, it vanishes (within the statistical uncertainty) at zero time, as observed in Figure 17 and in Table 5. For the same reason, $G_{xz}^{II,RotTr}(0)$ was found to be roughly zero in the three liquids.

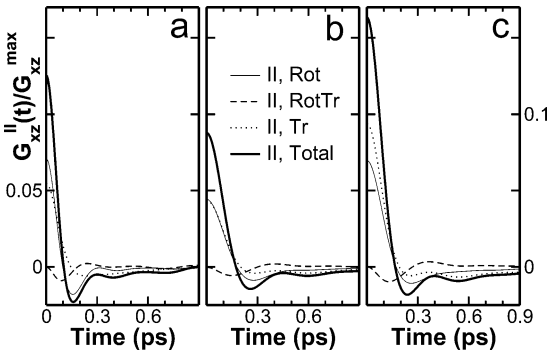

Figure 17. Contributions to the interaction-induced polarizability velocity TCF, $G_{xz}^{II}(t)/G_{xz}^{max}$, from rotational (Rot), translational (Tr), and the rotational-translational coupling (RotTr) components for (a) Bz, (b) HFB, and (c) TFB.

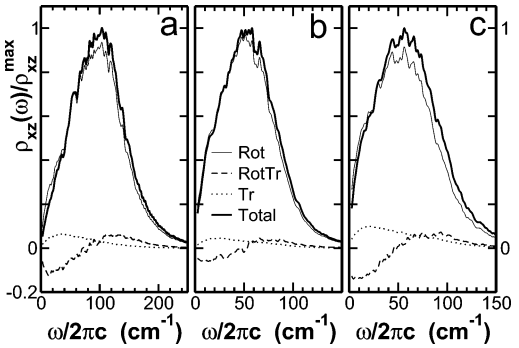

Figure 18. Rotational, translational, and cross contributions to $\rho_{xz}(\omega)$, the Fourier transform of $G_{xz}(t)$, for (a) Bz, (b) HFB, and (c) TFB.

The contributions of the different components of $G_{xz}(t)$ may also be analyzed in the frequency domain, by performing the Fourier−Laplace transform of $G_{xz}(t)$. To maintain a notation consistent with ref 29, we will denote the real part of the transform as

$$\rho_{xz}(\omega) = \mathrm{Re}\left[\int_0^\infty e^{i\omega t}\, G_{xz}(t)\, dt\right] \tag{33}$$

$\rho_{xz}(\omega)$ is usually referred to as the influence spectrum.[29] Equations 4, 16, and 33 imply that $\rho_{xz}(\omega)$ and the OKE susceptibility, $\chi''(\omega)$, are closely related and satisfy[29]

$$\chi''(\omega) \propto \frac{\rho_{xz}(\omega)}{\omega} \tag{34}$$

Figure 18 shows the contributions from rotational, translational, and cross RotTr degrees of freedom to the normalized influence spectra $\rho_{xz}(\omega)/\rho_{xz}^{max}$ obtained for the three liquids.

By inspecting Figure 18a, we see that here the relative intensity of the translational band is significantly reduced as compared to figure 3 of ref 29, where $\rho_{xz}(\omega)$ is shown for benzene. This is not unexpected because in ref 29 the center−center DID model for the interaction-induced polarizability was employed. Specifically, it has already been shown that the center−center DID model not only produces an underestimation of the orientational contribution to the polarizability dynamics

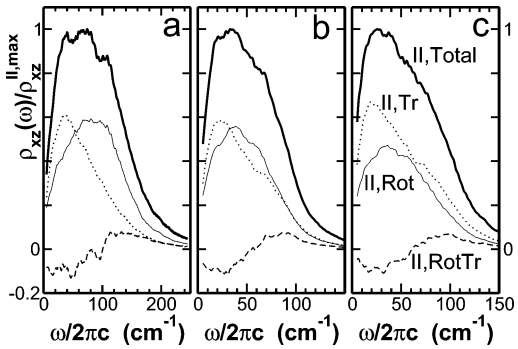

Figure 19. Rotational, translational, and cross contributions to the interaction-induced spectral density, $\rho_{xz}^{II}(\omega)$, or the Fourier transform of $G_{xz}^{II}(t)$, for (a) Bz, (b) HFB, and (c) TFB.

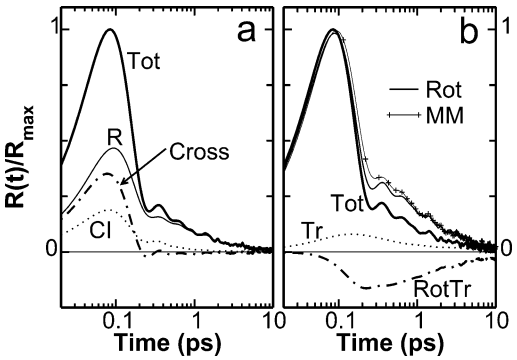

Figure 20. Contributions to the normalized nuclear response function, $R(t)/R_{max}$, from (a) the projection scheme and (b) obtained by integrating the polarizability velocity TCF $G_{xz}(t)$, for benzene.

but also overestimates the contribution from translational degrees of freedom.[25]

The translational band makes its main contribution to $\rho_{xz}(\omega)$ at very low frequencies, around 20−30 cm^{-1}, and is canceled in part by the negative rotation-translation coupling term, leaving as a result a dominant orientational contribution to the collective polarizability anisotropy.

Figure 19 shows how the interaction-induced influence spectrum, $\rho_{xz}^{II}(\omega)$, is built up from intermolecular translations and rotations, normalized with $\rho_{xz}^{II,max}(\omega)$, the maximum intensity of $\rho_{xz}^{II}(\omega)$.

The II-translational band has a maximum at 33, 28, and 20 cm^{-1} for Bz, HFB, and TFB, respectively. From the point of view of kinematics, because the molecular weight of TFB (132 amu) is intermediate between those of Bz (78 amu) and HFB (186 amu), one might have predicted that the maximum of the II-Tr band of TFB would be located between those corresponding to the other two liquids. Even though the difference is small, this is not the case here. We believe that the additional factor determining the II peak location in TFB is related to the strong preference of molecules in this liquid to form stacked parallel structures, which causes a slowing down in intermolecular translational dynamics, and therefore a shift toward lower frequencies in the maximum of the corresponding spectrum.

In Bz, the rotational band is noticeably shifted by about 90 cm^{-1} toward higher frequencies relative to the translational band. The shift is smaller in the other two liquids, on the order of 20 cm^{-1}. Regarding the relative intensities of II,Rot and II,Tr bands, in Bz both peaks have similar intensities, whereas in HFB the translational peak intensity exceeds by a small amount that of orientations, and in TFB the translational intensity at the maximum is roughly 40% greater than that of the orientational band. An interesting feature is present in $\rho_{xz}^{II,Tr}(\omega)$ of HFB and TFB, but absent from the corresponding Bz spectrum. Namely, in both liquids $\rho_{xz}^{II,Tr}(\omega)$ has a weak shoulder at $\omega/2\pi c \approx 70-80$ cm^{-1}, possibly because of translational intermolecular oscillations of neighbors in a local parallel arrangement.

D. Comparison between Projection Scheme and Steele Theory Results. Because the rotational, translational, and coupled contributions to the nuclear response function can be obtained from the Steele theory by performing a time integral of $G_{xz}(t)$ (eq 17), in this section we compare this way of separating different dynamical components of $R(t)$ to the projection scheme results described in Section II.A. In the former case, eq 17 was integrated using Simpson's rule and the resulting $R(t)$ has been calculated with a resolution of two integration time steps and evaluated up to 10 ps.

We chose to display the results for benzene, because the comparison yielded very similar features in the three liquids. Furthermore, we believe that the comparison shown here is a good representation not just for the set of Bz−HFB−TFB aromatic liquids but for a wider set of molecular liquids.

The most striking difference between these two approaches, shown in Figure 20, is the opposite sign of the cross term, which is positive at short times in the projection scheme and negative in the Steele approach. The positive sign in $R^{Cross}(t)$ can be understood by inspecting Figure 6. The orthogonality between the polarizability projected components Π^{R} and Π^{CI} at zero time imposes a condition for the initial value of the TCF, that is, $\psi_{xz}^{Cross}(0) \equiv 0$. At later times, this condition is relaxed if there is no clear separation in the time scales of reorientational and collision-induced dynamics. This coupling is usually negative for $t \neq 0$. It reflects the inability of the local structure around a molecule in a fluid to adjust instantaneously to changes in the orientation of that molecule.[18,25] Therefore, because all three projected components of $\psi_{xz}(t)$ have the same initial decreasing tendency with time, their time derivatives will have the same sign, yielding positive contributions to $R(t)$ at short times as a result.

As pointed out already, the projected reorientational contribution is given by $\psi_{xz}^{R}(t) = [(1 + f_{xz})^2 \psi_{xz}^{MM}(t)]$, which means that it has the same time dependence and a lower intensity that the molecular (MM) TCF. Thus, the maximum of $R^{R}(t)$ is by about a factor of 2 smaller than that of $R^{MM}(t)$. In the case of Steele results, $R^{MM}(t)$ and $R^{Rot}(t)$ look very similar, implying that the contribution from interaction-induced and cross MI correlations, $R^{II}(t)$ and $R^{MI}(t)$ to rotational dynamics is very small. Indeed, within the Steele approach, $R^{Tr}(t)$ and $R^{RotTr}(t)$ look very similar in shape to $R^{II}(t)$ and $R^{MI}(t)$, respectively (not shown). The Steele theory provides as well a natural extension of the INM theory beyond short time scales.[22]

Clearly, the two schemes yield quite different results. This is perhaps not surprising, given that in the projection scheme the orientational portion of Π_{xz}^{I} is identified as having the same time evolution as Π_{xz}^{M}, whereas the CI portion is orthogonal to it at $t = 0$. However, the Steele approach separates rotational and translational components based on the derivatives of $\mathbf{\Pi}$ with respect to translational and rotational coordinates, that is, identifies them as proportional to center-of-mass and angular velocities.

Figure 21 displays the contributions to the nuclear response function arising from interaction-induced correlations, $R^{II}(t)$, using the two schemes. The components of $R^{II}(t)$ look very different when analyzed according to the two approaches. In Figure 21a the maximum intensity of the projected collision-induced portion is almost 1.4 times larger than the reorientational part, whereas in panel b rotations and translations within the

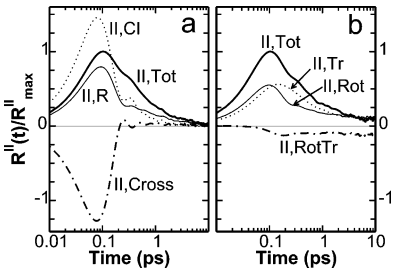

Figure 21. Contributions to the normalized nuclear response function from the interaction-induced polarizability, $R^{II}(t)/R^{II}_{max}$, using (a) the projection scheme and (b) the Steele approach, for benzene.

Steele scheme contribute almost equally to $R^{II}(t)$, consistent with the influence spectra shown in Figure 19a.

VI. Summary and Conclusions

We have studied the intermolecular dynamics and polarizability anisotropy relaxation in a set of aromatic liquids, Bz, HFB, and TFB, by MD simulations. A model in which the molecular polarizability is distributed over the carbon sites was employed, and first-order perturbation theory was used to represent the interaction-induced part of the collective polarizability. We investigated the effects of local structure on molecular and intermolecular dynamics and compared two commonly used methods of identifying the contributions of rotational and translational dynamics to the OKE response. We summarize our main findings here.

In agreement with the findings of Cabaço et al.,[10−12] our MD simulation data reveal that, despite the very similar molecular shapes, different charge distributions due to the different polarities of C−H and C−F bonds lead to a very different local intermolecular structure in TFB from the structures in Bz and HFB. Angular-radial pair distributions obtained from our MD simulations show that in TFB stacked parallel arrangements are strongly favored, whereas in the other two liquids perpendicular relative orientations of neighboring molecules are also quite likely.

We find that different local structures lead to significant differences in intermolecular dynamics in the three liquids. Local angular velocity CCFs show that in Bz and HFB molecules at short times rotate in directions opposite of those of their first-shell neighbors for both parallel and perpendicular arrangements of the sixfold axes, whereas in TFB, molecules in perpendicular arrangements rotate in phase with their neighbors and the extent of out-of-phase rotation of molecules in parallel arrangements is much smaller than that in the other two liquids.

Tao and Stratt[82] have investigated the structure, dynamics, and OKE response in a different class of aromatics: they have compared benzene to biphenyl (BP). The phenyl groups in BP have essentially the same structure, charge distribution, and polarizability as a benzene molecule but are geometrically constrained by a covalent C−C bond and a torsional potential. As a result, the local structure around each of the phenyl groups in liquid BP is very similar to the local structure in liquid benzene. Tao and Stratt found that the librational dynamics are also quite similar, accounting for the similarities in the reduced OKE responses[37] of the two liquids. Evidently, the effects of geometrical constraints in molecules containing multiple phenyl groups are quite different from the effects, considered here, of changes in the charge distribution in molecules with benzene-like geometry.

We have examined the effects of orientational pair correlations on the molecular portion of the polarizability anisotropy TCF, $\psi^{MM}_{xz}(t)$, by separating it into single-molecule and pair contributions, $\psi^{MMs}_{xz}(t)$ and $\psi^{MMp}_{xz}(t)$, and have analyzed it in terms of reorientation of molecules in different local environments. We found that $\psi^{MMp}_{xz}(t)$ exhibits a much slower decay rate than $\psi^{MMs}_{xz}(t)$, especially in Bz and HFB. Focusing on pairs within the first solvation shell, the rapidly decaying contributions to $\psi^{MMp}_{xz}(t)$ from molecules initially in parallel and perpendicular arrangements nearly cancel in Bz and HFB. In TFB, for which the average number of neighbors in parallel arrangements inside the first shell is the largest, the extent of cancellation is smaller. In all three liquids, the diffusive decay rates for pairs of molecules arranged in parallel configurations are lower than those for perpendicular pairs. The difference in the decay rates between parallel and perpendicular local pair correlations was found to be the largest in TFB, and the smallest in Bz.

We have used our data on $\psi^{MM}_{xz}(t)$ to determine how the shape of the ROKE spectra, that is, the OKE spectra from which the contribution of diffusive reorientation has been removed, is related to the local intermolecular structure. Loughnane et al.[39] have recently suggested that the lower-frequency peak in these spectra was due to molecules in parallel local arrangements, which for Bz and HFB correspond to inefficient packing relative the crystalline phase and the higher-frequency peak to perpendicular structures. However, we found that in all three liquids the band due to molecules in parallel arrangements actually peaks at a higher frequency than the band due to perpendicular local arrangements. We showed further that the relative peak positions of the two bands can be correlated with pair energy probability distributions that peak at a lower (i.e., more attractive) energy for parallel arrangements, indicating larger mean-squared torques and, therefore, higher librational frequencies should be expected for these arrangements.

The experimentally accessible ROKE spectrum contains contributions from translational modes in addition to nondiffusive orientational dynamics present in $\chi_{MM}''(\omega)$. Ryu and Stratt suggest, based on a scaling argument, that translational modes should be more important when the molecular isotropic polarizability is larger than the polarizability anisotropy.[29] Although the isotropic polarizabilities of Bz, HFB, and TFB are roughly identical (and always larger than the corresponding anisotropies), the polarizability anisotropies of HFB and TFB are somewhat larger than that of Bz. Therefore, the scaling argument would predict a smaller contribution from translations to the ROKE spectra of HFB and TFB than to Bz spectra. However, Loughnane et al. found excellent agreement between the Bz and benzene-d_6 ROKE spectra using a frequency scaling factor of $(k/I_{xx})^{1/2}$, where k is the force constant for the mode and I_{xx} is the moment of inertia for tumbling motions. Because this factor is proportional to the frequencies of single-molecule rotational modes, the authors conclude that translational modes would not play a significant role in the ROKE spectrum of benzene.[39] However, from the comparison between the computed ROKE total and orientational (local) $\chi''_{MM}(\omega)$ spectra, we found that there is a nonnegligible contribution from collision-induced and cross R−CI modes to the reduced susceptibility $\chi''(\omega)$ in the high-frequency portion of the spectrum, especially in Bz, bringing our results in closer agreement with the scaling argument of Ryu and Stratt.[29]

Two approaches, the Keyes−Kivelson projection scheme and the Steele theory, for which the projection into translational and rotational degrees of freedom is defined in the same way as in INM analysis, have been used to determine the dynamical origin of TCFs of collective variables in liquids. We have shown that

these methods yield quite different results when applied to the OKE response, $R(t)$, in the Bz, HFB, and TFB series of liquids and we expect that this is more generally true. This finding is perhaps not surprising, although it is important to be aware of this fact when drawing conclusions about the mechanisms of the OKE response.

The two methods of analysis provide different information, with the projection scheme more useful at long times and the Steele theory more useful at short times. Specifically, the projection scheme predicts the intensity of the component of $R(t)$ that is due to collective reorientation and makes it possible to show that the long-time decay of $R(t)$ is indeed due to reorientation, because it can be identified with the diffusive portion of $R^{R}(t) = [(1 + f_{xz})^2 R^{MM}(t)]$, as illustrated, for example, in Figure 20. Because $f_{xz} < 0$, we find that $R^{R}(t)$ is less intense than the pure molecular component $R^{MM}(t)$, a feature common to many other liquids.[23−25,83] Although the dynamical origin of $R^{R}(t)$ is clear, the remaining contributions to $R(t)$ in this scheme, $R^{CI}(t)$ and $R^{Cross}(t)$, do not have a dynamical origin that is as clearly identifiable, although one might be tempted to identify them as being due to translation and rotation-translation coupling, respectively. A better way to characterize them would be as originating from rapidly varying relaxation processes due to the presence of the interaction-induced polarizability.

The Steele theory, because it is based on the analysis of the polarizability anisotropy velocity TCF, $G_{xz}(t)$, can determine how polarizability anisotropy varies through the rate of change in translational and rotational molecular coordinates. At short times, the resulting components $G_{xz}^{Rot}(t)$, $G_{xz}^{Tr}(t)$, and $G_{xz}^{RotTr}(t)$ are nearly proportional to the corresponding velocity TCFs, given that polarizability derivatives with respect to molecular coordinates vary more slowly than molecular velocity components. Thus, on this scale the corresponding components of $R(t)$ have a relatively clear dynamical interpretation. However, at longer times, the time-scale separation between spatial polarizability derivatives and velocities no longer holds. On this scale, the Steele theory cannot identify the dynamical origin of $R(t)$ as being due to collective reorientation, with the constant local field factor $(1 + f_{xz})^2$ the only contribution of the interaction-induced polarizability.

What has perhaps not been evident earlier is the fact that the two schemes lead to splitting up the total OKE nuclear response, $R(t)$, into components that have quite different intensities and, especially in the case of the pairs $R^{CI}(t)$, $R^{Cross}(t)$ (projection scheme) and $R^{Tr}(t)$, $R^{RotTr}(t)$ (Steele theory), very different time dependence. This makes it difficult to unambiguously determine how dynamical processes associated with the fluctuations in the interaction-induced polarizability contribute to the OKE response.

Acknowledgment. We wish to thank Professor John T. Fourkas for kindly sharing with us his results on optical Kerr-effect experiments in aromatic liquids prior to publication, for providing us the experimental OKE data on TFB, and for many inspiring and illuminating discussions. We also like to thank the reviewer for valuable comments and a very careful reading of our manuscript. This work was supported in part by the National Science Foundation, grants CHE 9981539 and CHE 0608640.

Appendix A

Time Derivative of the Collective Polarizability in the First-Order Site−Site Model. The time derivative of the collective polarizability (eq 5) involves evaluating the time derivatives, $\dot{\boldsymbol{\alpha}}_i$, of unperturbed molecular polarizabilities, and $\dot{\boldsymbol{\pi}}(ij)$, the derivatives of pair interaction terms. Because $\boldsymbol{\alpha}_i$ for rigid symmetric-top molecules depends only on orientational vectors (eq 8), its time derivative gives rise to a purely rotational contribution, given by

$$\dot{\alpha}_{i,\alpha\beta} = \gamma_0 (u_{i,\alpha}\, l^{\mathbf{u}}_{i,\beta} + l^{\mathbf{u}}_{i,\alpha}\, u_{i,\beta}) \tag{A.1}$$

where the Greek subindices represent the Cartesian components x, y, and z and[28]

$$\mathbf{l}^{\mathbf{u}}_i \equiv \frac{\mathrm{d}\hat{\mathbf{u}}_i}{\mathrm{d}t} = \boldsymbol{\omega}_i \times \hat{\mathbf{u}}_i \tag{A.2}$$

where $\boldsymbol{\omega}_i$ is the angular velocity of molecule i.

The time derivative of the interaction-induced terms, $\boldsymbol{\pi}(ij)$, given by eq 6, will give rise to three terms

$$\dot{\boldsymbol{\pi}}(ij) = \sum_{mn}^{6} \{(\dot{\boldsymbol{\alpha}}_{im} \cdot \mathbf{T}^{(2)}_{imjn} \cdot \boldsymbol{\alpha}_{jn} + \boldsymbol{\alpha}_{im} \cdot \mathbf{T}^{(2)}_{imjn} \cdot \dot{\boldsymbol{\alpha}}_{jn}) + \boldsymbol{\alpha}_{im} \cdot \dot{\mathbf{T}}^{(2)}_{imjn} \cdot \boldsymbol{\alpha}_{jn}\} \tag{A.3}$$

where $\mathbf{T}^{(2)}_{imjn} \equiv \mathbf{T}^{(2)}(\mathbf{r}_{im,jn})$. The terms inside parentheses are a purely rotational contribution, because within the site−site model employed in this work, the effective polarizabilities, $\boldsymbol{\alpha}_{im}$, given by eq 9, depend only on orientational vectors. Thus, the expression for $\dot{\boldsymbol{\alpha}}_{im}$ is given by eq A.1, in which γ_0 is replaced with $\gamma_{0,m}$.

The time derivative of the site−site dipole tensor, $\dot{\mathbf{T}}^{(2)}_{imjn}$, is calculated in detail in Appendix B. Given that $\mathbf{T}^{(2)}_{imjn}$ depends on the intermolecular site−site vector, $\mathbf{r}_{im,jn}$, we anticipate that its derivative will give rise to rotational and translational contributions, which we denote as $\dot{\mathbf{T}}^{(2)}_{Rot}$ and $\dot{\mathbf{T}}^{(2)}_{Tr}$.

Then, putting all terms together, we have for the rotational component of the collective polarizability velocity

$$\dot{\boldsymbol{\Pi}}^{Rot} = \sum_{i}^{N} \dot{\boldsymbol{\alpha}}_i + \sum_{i,j\neq i}^{N} \sum_{mn}^{6} \{(\dot{\boldsymbol{\alpha}}_{im} \cdot \mathbf{T}^{(2)}_{imjn} \cdot \boldsymbol{\alpha}_{jn} + \boldsymbol{\alpha}_{im} \cdot \mathbf{T}^{(2)}_{imjn} \cdot \dot{\boldsymbol{\alpha}}_{jn}) + \boldsymbol{\alpha}_{im} \cdot \dot{\mathbf{T}}^{(2)}_{Rot} \cdot \boldsymbol{\alpha}_{jn}\} \tag{A.4}$$

and the translational component is given by

$$\dot{\boldsymbol{\Pi}}^{Tr} = \sum_{i,j\neq i}^{N} \sum_{mn}^{6} \boldsymbol{\alpha}_{im} \cdot \dot{\mathbf{T}}^{(2)}_{Tr} \cdot \boldsymbol{\alpha}_{jn} \tag{A.5}$$

Appendix B

Time Derivative of the Site−Site Dipole Tensor. To perform the time derivative of the site−site dipole tensor, we should first identify the three unit vectors, $\hat{\mathbf{u}}_i$, $\hat{\mathbf{v}}_i$, and $\hat{\mathbf{w}}_i$, defining the orientation of the ith molecule. They are displayed in Figure 22.

Because the molecule is planar, the carbon coordinates of molecule i, $\mathbf{r}_{im}$, can be written in terms of the center-of-mass coordinates, that we will denote explicitly with a "com" superscript label, $\mathbf{r}^{com}_i$, plus a linear combination of the in-plane unit vectors $\hat{\mathbf{v}}_i$ and $\hat{\mathbf{w}}_i$

$$\mathbf{r}_{im} = \mathbf{r}^{com}_i + a_{vm}\hat{\mathbf{v}}_i + a_{wm}\hat{\mathbf{w}}_i \tag{B.1}$$

where the scalars a_{vm} and a_{wm} represent the projections along

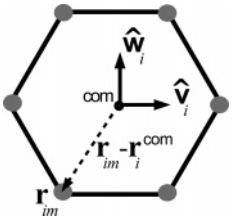

Figure 22. Scheme of the aromatic molecules studied, with the orientational vectors $\hat{\mathbf{v}}_i$ and $\hat{\mathbf{w}}_i$ displayed; $\hat{\mathbf{u}}_i$ is perpendicular to the molecular plane and is not plotted. Gray circles indicate carbon sites, where the effective polarizabilities, α_{im}, are located in the site−site model.

$\hat{\mathbf{v}}_i$ and $\hat{\mathbf{w}}_i$ of the vectors connecting the center-of-mass to the mth carbon site, $(\mathbf{r}_{im} - \mathbf{r}_i^{com})$

$$a_{vm} = (\mathbf{r}_{im} - \mathbf{r}_i^{com})\cdot\mathbf{v}_i \tag{B.2}$$

$$a_{wm} = (\mathbf{r}_{im} - \mathbf{r}_i^{com})\cdot\mathbf{w}_i \tag{B.3}$$

Using eq B.1 for the site−site separation vector, we obtain

$$\mathbf{r}_{im,jn} = \mathbf{r}_{ij}^{com} + a_{vm}\hat{\mathbf{v}}_i + a_{wm}\hat{\mathbf{w}}_i - a_{vn}\hat{\mathbf{v}}_j - a_{wn}\hat{\mathbf{w}}_j \tag{B.4}$$

where the dependence of $\mathbf{r}_{im,jn}$ on the center-of-mass separation and on the orientational vectors of the pair involved, that is, $\hat{\mathbf{v}}_i$, $\hat{\mathbf{v}}_j$, $\hat{\mathbf{w}}_i$, and $\hat{\mathbf{w}}_j$, has been put in an explicit way. Then, using the chain rule to differentiate $\mathbf{T}^{(2)}(\mathbf{r})$, it yields

$$\dot{\mathbf{T}}^{(2)}(\mathbf{r}_{im,jn}) = \frac{\partial \mathbf{T}^{(2)}(\mathbf{r}_{im,jn})}{\partial \mathbf{r}_{im,jn}} \cdot \frac{\partial \mathbf{r}_{im,jn}}{\partial t} \tag{B.5}$$

with

$$\frac{\partial \mathbf{r}_{im,jn}}{\partial t} = \frac{\partial \mathbf{r}_{im,jn}}{\partial \mathbf{r}_{ij}^{com}} \cdot \frac{d\mathbf{r}_{ij}^{com}}{dt} + \frac{\partial \mathbf{r}_{im,jn}}{\partial \hat{\mathbf{v}}_i} \cdot \frac{d\hat{\mathbf{v}}_i}{dt} + \frac{\partial \mathbf{r}_{im,jn}}{\partial \hat{\mathbf{w}}_i} \cdot \frac{d\hat{\mathbf{w}}_i}{dt} + \frac{\partial \mathbf{r}_{im,jn}}{\partial \hat{\mathbf{v}}_j} \cdot \frac{d\hat{\mathbf{v}}_j}{dt} + \frac{\partial \mathbf{r}_{im,jn}}{\partial \hat{\mathbf{w}}_j} \cdot \frac{d\hat{\mathbf{w}}_j}{dt} \tag{B.6}$$

The insertion of eq B.6 into eq B.5 can be put in a more compact form by noting that

$$\partial \mathbf{T}^{(2)}(\mathbf{r})/\partial \mathbf{r} = \mathbf{T}^{(3)}(\mathbf{r}) \tag{B.7}$$

$$\partial \mathbf{r}_{im,jn}/\partial \mathbf{r}_{ij}^{com} = \mathbf{1} \tag{B.8}$$

$$d\mathbf{r}_{ij}^{com}/dt = \boldsymbol{v}_{ij}^{com} \tag{B.9}$$

$$\partial \mathbf{r}_{im,jn}/\partial \hat{\mathbf{v}}_i = a_{vm}\mathbf{1} \tag{B.10}$$

$$\partial \mathbf{r}_{im,jn}/\partial \hat{\mathbf{w}}_i = a_{wm}\mathbf{1} \tag{B.11}$$

$$\partial \mathbf{r}_{im,jn}/\partial \hat{\mathbf{v}}_j = -a_{vn}\mathbf{1} \tag{B.12}$$

$$\partial \mathbf{r}_{im,jn}/\partial \hat{\mathbf{w}}_j = -a_{wn}\mathbf{1} \tag{B.13}$$

$$d\hat{\mathbf{v}}_i/dt \equiv \mathbf{l}_i^v = \boldsymbol{\omega}_i \times \hat{\mathbf{v}}_i \tag{B.14}$$

$$d\hat{\mathbf{w}}_i/dt \equiv \mathbf{l}_i^w = \boldsymbol{\omega}_i \times \hat{\mathbf{w}}_i \tag{B.15}$$

Thus, inserting eq B.6 into B.5 and using the relations B.7−B.15, we obtain

$$\dot{\mathbf{T}}^{(2)}(\mathbf{r}_{im,jn}) = \mathbf{T}^{(3)}(\mathbf{r}_{im,jn})\cdot\boldsymbol{v}_{ij}^{com} + [\mathbf{T}^{(3)}(\mathbf{r}_{im,jn})\cdot(a_{vm}\mathbf{l}_i^v + a_{wm}\mathbf{l}_i^w - a_{vn}\mathbf{l}_j^v - a_{wn}\mathbf{l}_j^w)] \tag{B.16}$$

The first term in eq B.16 depends on the relative center-of-mass linear velocity, giving rise to a translational contribution, denoted as $\dot{\mathbf{T}}_{Tr}^{(2)}$ in Appendix A. The term inside square brackets depends on the orientational velocities, providing the rotational contribution that is absent from the center−center model of $\boldsymbol{\pi}(ij)$, and is denoted as $\dot{\mathbf{T}}_{Rot}^{(2)}$.

References and Notes

(1) Narten, A. H. *J. Chem. Phys.* **1977**, *67*, 2102.
(2) Narten, A. H. *J. Chem. Phys.* **1968**, *48*, 1630.
(3) Bartsch, E.; Bertagnolli, H.; Chieux, P. *Ber. Bunsen-Ges. Phys. Chem.* **1986**, *90*, 34.
(4) Cabaço, M. I.; Danten, Y.; Besnard, M.; Guissani, Y.; Guillot, B. *J. Phys. Chem. B* **1997**, *101*, 6977.
(5) Elola, M. D.; Ladanyi, B. M. *J. Chem. Phys.* **2005**, *123*, 224508.
(6) Chelli, R.; Cardini, G.; Procaci, P.; Righini, R.; Califano, S.; Albrecht, A. *J. Chem. Phys.* **2000**, *113*, 6851.
(7) Chelli, R.; Cardini, G.; Ricci, M.; Bartolini, P.; Righini, R.; Califano, S. *Phys. Chem. Chem. Phys.* **2001**, *3*, 2803.
(8) Battaglia, M. R.; Buckingham, A. D.; Williams, J. H. *Chem. Phys. Lett.* **1981**, *78*, 421.
(9) Vrbancich, J.; Ritchie, G. L. D. *J. Chem. Soc., Faraday Trans. 2* **1980**, *76*, 648.
(10) Cabaço, M. I.; Danten, Y.; Besnard, M.; Guissani, Y.; Guillot, B. *Chem. Phys. Lett.* **1996**, *262*, 120.
(11) Cabaço, M. I.; Tassaing, T.; Danten, Y.; Besnard, M. *Chem. Phys. Lett.* **2000**, *325*, 163.
(12) Cabaço, M. I.; Tassaing, T.; Danten, Y.; Besnard, M. *J. Phys. Chem. A* **2000**, *104*, 10986.
(13) Fourkas, J. T. *Ultrafast Infrared and Raman Spectroscopy*; Fayer, M. D., Ed.; Marcel Dekker: New York, 2001.
(14) Smith, N. A.; Meech, S. R. *Int. Rev. Phys. Chem.* **2002**, *21*, 75.
(15) Righini, R. *Science* **1993**, *262*, 1386.
(16) Berne, B. J.; Pecora, R. *Dynamic Light Scattering with Applications to Chemistry, Biology, and Physics*; Dover: New York, 2000.
(17) Madden, P. A. *Molecular Liquids: Dynamics and Interactions*; Barnes, A. J., Orville-Thomas, W. J., Yarwood, J., Eds.; NATO-ASI Series C135: Reidel: Dordrecht, 1984.
(18) Frenkel, D.; McTague, J. P. *J. Chem. Phys.* **1980**, *72*, 2801.
(19) Geiger, L. C.; Ladanyi, B. M. *Chem. Phys. Lett.* **1989**, *159*, 413.
(20) Stassen, H.; Dorfmüller, T.; Ladanyi, B. M. *J. Chem. Phys.* **1994**, *100*, 6318.
(21) Geiger, L. C.; Ladanyi, B. M. *J. Chem. Phys.* **1987**, *87*, 191.
(22) Ladanyi, B. M.; Klein, S. *J. Chem. Phys.* **1996**, *105*, 1552.
(23) Ladanyi, B. M.; Liang, Y. Q. *J. Chem. Phys.* **1995**, *103*, 6325.
(24) Paolantoni, M.; Ladanyi, B. M. *J. Chem. Phys.* **2002**, *117*, 3856.
(25) Elola, M. D.; Ladanyi, B. M. *J. Chem. Phys.* **2005**, *123*, 224506; note that the expression following eq 7 in this article should read $\Pi = \Pi^{M,\bar{\alpha}} + \Pi^{M,\gamma} + \Pi^{I,\bar{\alpha}\bar{\alpha}} + \Pi^{I,\bar{\alpha}\gamma} + \Pi^{I,\gamma\gamma}$.
(26) Keyes, T.; Kivelson, D. *J. Chem. Phys.* **1972**, *56*, 1057.
(27) Steele, W. A. *Mol. Phys.* **1987**, *61*, 1031.
(28) Stassen, H.; Steele, W. A. *J. Chem. Phys.* **1999**, *110*, 7382.
(29) Ryu, A.; Stratt, R. M. *J. Phys. Chem. B* **2004**, *108*, 6782.
(30) Keyes, T. *J. Chem. Phys.* **1996**, *104*, 9349.
(31) Keyes, T. *J. Phys. Chem. A* **1997**, *101*, 2921.
(32) Ladanyi, B. M.; Stratt, R. M. *J. Phys. Chem.* **1995**, *99*, 2502.
(33) McMorrow, D.; Lotshaw, W. T. *Chem. Phys. Lett.* **1993**, *201*, 369.
(34) Smith, N. A.; Lin, S. J.; Meech, S. R.; Shirota, H.; Yoshihara, K. *J. Phys. Chem. A* **1997**, *101*, 9578.
(35) Smith, N. A.; Lin, S. J.; Meech, S. R.; Yoshihara, K. *J. Phys. Chem. A* **1997**, *101*, 3641.
(36) Chang, Y. J.; Castner, E. W., Jr. *J. Phys. Chem.* **1996**, *100*, 3330.
(37) Rajian, J. R.; Hyun, B. R.; Quitevis, E. L. *J. Phys. Chem. A* **2004**, *108*, 10107.
(38) Neelakandan, M.; Pant, D.; Quitevis, E. L. *J. Phys. Chem. A* **1997**, *101*, 2936.
(39) Loughnane, B. J.; Scodinu, A.; Fourkas, J. T. *J. Phys. Chem. B* **2006**, *110*, 5708.
(40) Skaf, M. S.; Vechi, S. M. *J. Chem. Phys.* **2003**, *119*, 2181.
(41) Stassen, H.; Dorfmüller, T. *Ber. Bunsen-Ges. Phys. Chem.* **1991**, *95*, 995.
(42) Keyes, T.; Ladanyi, B. M. *Mol. Phys.* **1977**, *33*, 1271.
(43) Ladanyi, B. M.; Keyes, T. *J. Chem. Phys.* **1978**, *68*, 3217.
(44) Ladanyi, B. M. *J. Chem. Phys.* **1983**, *78*, 2189.
(45) Geiger, L. C.; Ladanyi, B. M.; Chapin, M. E. *J. Chem. Phys.* **1990**, *93*, 4533.
(46) Mossa, S.; Ruocco, G.; Sampoli, M. *J. Chem. Phys.* **2002**, *117*, 3289.
(47) Elola, M. D.; Ladanyi, B. M.; Scodinu, A.; Loughnane, B. J.; Fourkas, J. T. *J. Phys. Chem. B* **2005**, *109*, 24085.

(48) Thole, B. T. *Chem. Phys.* **1981**, *59*, 341.
(49) van Duijnen, P. T.; Swart, M. *J. Phys. Chem. A* **1998**, *102*, 2399.
(50) Alms, G. R.; Burnham, A. K.; Flygare, W. H. *J. Chem. Phys.* **1975**, *63*, 3321.
(51) Gentle, I. R.; Ritchie, G. L. D. *J. Phys. Chem.* **1989**, *93*, 7740.
(52) Gray, C. G.; Gubbins, K. E. *Theory of Molecular Fluids*; Clarendon Press: Oxford, 1984; Vol. 1.
(53) Sonoda, M. T.; Vechi, S. M.; Skaf, M. S. *Phys. Chem. Chem. Phys.* **2005**, *7*, 1176−1180.
(54) Steele, W.; Stassen, H. *J. Mol. Liq.* **2002**, *98*, 303.
(55) Williams, D. E.; Cox, S. R. *Acta Crystallogr.* **1984**, *B40*, 404.
(56) Williams, D. E.; Houpt, D. J. *Acta Crystallogr.* **1986**, *B42*, 286.
(57) Hogenboom, D. L.; Krynicki, K.; Sawyer, D. W. *Mol. Phys.* **1980**, *40*, 823.
(58) Ciccotti, G.; Ferrario, M.; Ryckaert, J. P. *Mol. Phys.* **1982**, *47*, 1253.
(59) Verlet, L. *Phys. Rev.* **1967**, *159*, 98.
(60) Allen, M. P.; Tildesley, D. J. *Computer Simulation of Liquids*; Oxford University Press: New York, 1994.
(61) Ryckaert, J. P.; Ciccotti, G.; Berendsen, H. J. C. *J. Comput. Phys.* **1977**, *23*, 327.
(62) Danten, Y.; Cabaço, M. I.; Tassaing, T.; Besnard, M. *J. Chem. Phys.* **2001**, *115*, 4239.
(63) Balucani, U.; Vallauri, R.; Murthy, C. S. *J. Chem. Phys.* **1982**, *77*, 3233.
(64) Balucani, U.; Vallauri, R.; Murthy, C. S.; Gaskell, T.; Woolfson, M. S. *J. Phys. C* **1983**, *16*, 5605.
(65) Endo, Y.; Endo, H. *J. Chem. Phys.* **1984**, *80*, 2087.
(66) Verdaguer, A.; Padró, J. A. *Phys. Rev. E* **2000**, *62*, 532.
(67) Hirata, Y. *J. Phys. Chem. A* **2002**, *106*, 2187.
(68) Verdaguer, A.; Padró, J. A. *J. Chem. Phys.* **2001**, *114*, 2738.
(69) Verdaguer, A.; Padró, J. A. *Mol. Phys.* **2002**, *100*, 3401.
(70) Verdaguer, A.; Padró, J. A. *J. Chem. Phys.* **1998**, *109*, 228.
(71) Madden, P. A.; Tildesley, D. J. *Mol. Phys.* **1985**, *55*, 969.
(72) Kivelson, D.; Madden, P. A. *Annu. Rev. Phys. Chem.* **1980**, *31*, 523.
(73) Jannelli, M. P.; Magazu, S.; Migliardo, P.; Aliotta, F.; Tettamanti, E. *J. Phys.: Condens. Matter* **1996**, *8*, 8157.
(74) Bauer, D. R.; Brauman, J. I.; Pecora, R. *J. Chem. Phys.* **1975**, *63*, 53.
(75) Vrbancich, J.; Ritchie, G. L. D. *Chem. Phys. Lett.* **1983**, *94*, 63.
(76) Battaglia, M. R.; Cox, T. I.; Madden, P. A. *Mol. Phys.* **1979**, *37*, 1413.
(77) Brown, N. M. D.; Maguire, J. F.; Swinton, F. L. *Faraday Discuss. Chem. Soc.* **1978**, 244.
(78) Burnham, A. K.; Alms, G. R.; Flygare, W. H. *J. Chem. Phys.* **1975**, *62*, 3289.
(79) Chang, Y. J.; Castner, E. W., Jr. *J. Chem. Phys.* **1993**, *99*, 113.
(80) Vöhringer, P.; Scherer, N. F. *J. Phys. Chem.* **1995**, *99*, 2684.
(81) Jeffrey, G. A.; Ruble, J. R.; McMullan, R. K.; Pople, J. A. *Proc. R. Soc. A* **1987**, *414*, 47.
(82) Tao, G.; Stratt, R. M. *J. Phys. Chem. B* **2006**, *110*, 976.
(83) Kiyohara, K.; Kamada, K.; Ohta, K. *J. Chem. Phys.* **2000**, *112*, 6338.